A high-fat diet enriched in medium chain triglycerides triggers hepatic thermogenesis and improves metabolic health in lean and obese mice

Sabri Ahmed Rial, Antoine Jutras-Carignan, Karl-Frédérik Bergeron, Catherine Mounier
Molecular Metabolism of Lipids Laboratory, Biological Sciences Department, University of Quebec at Montreal (UQAM)

*** To whom correspondence should be addressed:** Catherine Mounier, Biological Sciences Department, UQAM, 141 President-Kennedy Avenue, Montreal (Quebec), Canada H2X 1Y4, 1-514-897-3000 extension 8912, mounier.catherine@uqam.ca

Author contributions: CM, SAR and KFB designed the project. SAR performed most experiments. AJC optimized then performed the cell culture experiments and participated to their interpretation (**Fig.3H**). SAR and KFB wrote the manuscript. KFB and CM edited the manuscript.

HIGHLIGHTS:

- Medium chain triglycerides (MCT) drastically deplete hepatic lipid droplets and white adipose tissues.
- MCT improve body weight and insulin sensitivity in healthy and in obese mice.
- MCT induce thermogenic features in liver.
- FFAR1/GPR40 is required for induction of Ucp1 by MCT in hepatocytes.

ABSTRACT

Obesity, liver steatosis and type 2 diabetes are major diseases partly imputed to energy-dense diets rich in long chain triglycerides (LCT). The search for bioactive nutrients that help to overcome metabolic diseases is a growing field. In this regard, medium chain triglycerides (MCT) were shown to promote lipid catabolism and to stimulate brown adipose tissue thermogenesis. The objective of our study was to evaluate if the replacement of LCT by MCT in high-fat diets could prevent and/or reduce metabolic disorders. For this purpose, two cohorts of C57BL/6 mice were fed during 10 weeks with three isocaloric high-fat diets with variable MCT content. Cohort A was composed of lean mice while cohort B was composed of obese, insulin resistant mice. In cohort A, replacement of LCT by MCT preserved metabolic health, in part by triggering hepatic thermogenesis. We further found that medium chain fatty acids promote thermogenesis markers within cultured hepatocytes in a FFAR1/GPR40-dependent manner. In cohort B, high-fat diets enriched in MCT promoted body fat depletion and caused metabolic health improvement, together with the induction of thermogenesis markers in the liver as well as in subcutaneous white adipose tissue. Our study supports that replacement of LCT by MCT in high-fat diets improve the metabolic features associated with obesity.

KEYWORDS: Obesity; liver steatosis; insulin resistance; medium chain triglycerides; UCP1; FFAR1/GPR40.

1. INTRODUCTION

Lipid anabolism includes dietary lipid assimilation, via intestinal then peripheral fatty acid uptake, and endogenous lipid biosynthesis via *de novo* lipogenesis (DNL) (1, 2). DNL converts excess of acetyl-CoA (produced by oxidation of high amounts of carbohydrates and lipids) into fatty acids. These latter mostly undergo esterification into triglycerides for long-term energy storage within lipid droplets (LD) and for systemic lipoprotein trafficking (1, 2). On the other hand, the lipid catabolism coordinates lipolysis, which consists in triglyceride hydrolyzation into free fatty acids, with peroxisomal and mitochondrial β-oxidation of fatty acids to yield chemical energy (ATP) and heat (3, 4).

Within metabolically active cells, lipid homeostasis is tightly regulated (5) for example by the widely conserved AMP-activated protein kinase (AMPK) (6, 7). When activated by an increase in AMP relative to ATP (corresponding to a low energy state), AMPK directly triggers lipid catabolism (6-9). Conversely, a decrease in the AMP:ATP ratio lowers AMPK activity, favoring lipid anabolism (6, 7).

Obesity, an alarmingly prevalent condition (10), results from metabolic imbalance caused by abnormally sustained lipid anabolism. Typically reflected by white adipose tissue (WAT) expansion (11) as well as by ectopic deposition of fats (11, 12), obesity is a strong contributor to metabolic diseases such as type 2 diabetes (10, 13) and liver steatosis (14-16). Long chain fatty acids (LCFA) , that constitute the vast majority of common dietary fats (17, 18), are well documented to trigger such deleterious anabolic imbalance (19-26).

One emerging strategy to overcome obesity and associated disorders consists in the stimulation of non-shivering thermogenesis (27-32) of metabolically active tissues such as brown and beige adipose tissues (BAT) (33) as well as skeletal muscle (34). Activation of thermogenesis involves the biosynthesis of mitochondria overexpressing the uncoupling protein 1 (UCP1) that actively dissipates a part of chemical energy into heat (27, 35).

Several bioactive compounds have been characterized as potent inducers of thermogenesis in BAT and WAT (28-32). Recently, dietary medium chain triglycerides

(MCT) have been shown to activate thermogenic features at the level of the interscapular BAT (36, 37). MCT are esterified saturated fatty acids with chain lengths not exceeding ten carbon atoms, called medium chain fatty acids (MCFA) (38-40). Concentrated MCT oils consist usually of esterified octanoic (C8) and decanoic (C10) acids (40). MCFA undergo a metabolism that is distinct from LCFA (41). In brief, dietary MCFA are transported to the liver via the hepatic portal blood system independently of chylomicron trafficking, and their translocation across mitochondrial membranes is not rate-limited by the carnitine palmitoyltransferase (CPT) system (42, 43). These properties allow MCFA to be mainly metabolized by the liver, where they preferentially undergo a not rate-limiting mitochondrial β-oxidation instead of re-esterification (42, 43). We previously demonstrated that, contrary to LCFA, MCFA do not induce triglyceride accumulation within hepatocytes, and better promote lipid catabolism. MCFA also improve insulin sensitivity by increasing basal and insulin-induced phosphorylation of the AKT-mTOR insulin signaling pathway (21). MCFA have otherwise been reported to activate PPARγ (44) and FFAR1/GPR40 (45) pathways.

In the present study, we showed that dietary fat in the form of MCT lead to global metabolic health improvement in lean as well as in obese mice. Dietary MCT noticeably triggered thermogenic features in the liver, and also tended to induce them in subcutaneous WAT. This provides new insight on the metabolically beneficial bioactive properties of MCT.

2. MATERIALS AND METHODS

2.1. Mice and diets

Three-week old male C57BL/6 mice (Charles River laboratories, Canada) were acclimated to our animal facilities during two weeks prior to diet protocols. Mice were continuously housed, 4 per cage at 24±1°C in a 12h light/dark cycle, with free access to water. UQAM's animal care committee approved all experimental procedures (CIPA protocol 780).

Four diets, whose caloric breakdown and nutritional composition are detailed in **Table 1**, were used (Research Diets, USA): i- a standard low-fat diet (LFD; cat. #D12450H) with 10% kcal from fat (5% from lard LCT and 5% from soy oil LCT); ii- a standard high-fat diet (HFD; cat. #D12451) with 45% kcal from fat (40% from lard LCT and 5% from soy oil LCT); iii- a customized high-fat diet (M20) with 45% kcal from fat (20% from MCT, 20% from lard LCT and 5% from soy oil LCT); and iv- a second customized high-fat diet (M40) with 45% kcal from fat (40% from MCT and 5 % from soy oil LCT). The diet manufacturer used plant-based Dermol M-5 (ALZO international Inc.) MCT oil, containing 60% C8 and 40% C10, to produce our modified diets.

A first cohort of 32 mice (designated as cohort A) was divided in 4 groups of 8 mice and continuously fed *ad-libitum* with either LFD, HFD, M20 or M40 diets for 10 weeks. A second cohort of 32 mice (cohort B) was first fed with HFD for 10 weeks to induce obesity and insulin resistance, then divided in 4 groups of 8 mice and fed LFD, HFD, M20 or M40 diets for 10 more weeks.

Mice were euthanized after a 6h diurnal fast and plasma samples were stored at -20°C for future analyses. Whole livers, and WAT samples (dorsal subcutaneous, epididymal) were flash-frozen in liquid nitrogen and stored at -80°C.

2.2. Body weight, food and energy intake

Individual body weight was monitored weekly and weight change was calculated as a percentage of the reference weight measured at week 0 in cohort A and at week 10 in cohort B. Food consumption in each cage was monitored daily, during 10 weeks on the experimental diets, as the difference (in grams) between the food supplied and the quantity of food remaining divided by the number of animals per cage. Individual energy intake was calculated as the product of food intake and energy content of diets (see **Table 1**). Areas under curve (AUC) of energy intake (in kcal) as function of time (in weeks) were computed using the trapezoidal function of the GraphPad software. At the end of the 10-week diet period, the food efficiency ratio was calculated by dividing weight gain per total food intake.

2.3. Glucose homeostasis

Glycemia measurement, glucose tolerance tests (GTT) and insulin tolerance tests (ITT) were assessed after a 6h diurnal fast. Blood glucose concentration was measured on 2µl of tail vein blood using an Accu-Chek Aviva glucometer (Roche). For GTT, glycemia was evaluated at time-points -15, 0, 15, 30, 60, 90 and 120 min where 0 was the time of intraperitoneal D-(+)-Glucose injection (1 g/kg body weight; Sigma-Aldrich, cat. #G8270). For ITT, glycemia was evaluated at time-points -15, 0, 15, 30, 45, 60 and 90 min where 0 was the time of intraperitoneal injection of human recombinant insulin (0.5 U/kg body weight; ThermoFisher Scientific, cat. #12585-014). Data are presented as AUC of blood glucose concentration as function of time (in minutes). In cohort A, GTT and ITT were performed at weeks 8 and 9 respectively. Homeostasis model assessment of insulin resistance (HOMA-IR) was calculated from plasma samples as follow: [glycemia (mM) x insulinemia (ng/ml)] / 22.5. In cohort B, GTT were performed at week 0, 8 and 18, while ITT were performed at weeks 9 and 19. Note that the week 0 and 8 GTT confirmed HFD-induced glucose intolerance before the diet switch.

2.4. Circulating markers

Circulating markers were measured from plasma samples. Fasting insulinemia and leptinemia were quantified using ELISA kits (Crystal Chem, cat. #90080 and cat. #90030), and triglyceridemia was quantified using a colorimetric assay kit (Cayman Chemical, cat. #10010303-96), according to the manufacturer's protocols.

2.5. Histology

Liver and WAT (subcutaneous and epididymal) samples were fixed in Bouin's solution (75% saturated picric acid, 7.5% formaldehyde, 5% glacial acetic acid) overnight at room temperature prior to paraffin embedding. Liver microtome sections (8 µm) were stained with Masson's trichrome while adipose tissue microtome sections (8 µm) were stained with hematoxylin and eosin. Samples were visualized under white light using a Nikon Eclipse Ti microscope equipped with a Scion CFW-1612C color-camera. LD size and area within liver sections, as well as adipocyte size, were measured using the Particle Analysis function of the ImageJ software, after the conversion of images into binary format. For LD measurements, the Particle Analysis function has been set to consider LD

with a sphericity coefficient of 0.7-1.0 and a size range of 0.07-2000 μm^2, thus excluding vessels and artefacts.

2.6. Western blots

Total proteins were extracted from liver samples with a RIPA buffer (50 mM Hepes, 125 mM NaCl, 100 mM NaF, 10 mM Na-pyrophosphate, 10% glycerol, 1% Triton X-100, 1.5 mM MgCl2, 1 mM ethylene glycol-bis(2-aminoethylether)-N,N,N′,N′-tetraacetic acid, 2 mM Na-orthovanadate, 1.5 mM PMSF, 1× cOmplete protease inhibitors, pH 7.2). Protein concentration was determined by the Bradford method (46), then diluted at 1 μg/μL in Laemmli buffer (50 mM Tris-HCl at pH 6.8, 5% β-mercaptoethanol, 2% sodium dodecyl sulfate (SDS), 0.01% bromophenol blue, 10% glycerol) before denaturation (5 min at 95°C). Denatured proteins (20 μg) were loaded onto SDS-PAGE, and immunoblot analyses were carried out using the primary antibodies (**Table 2)**. Horseradish peroxidase (HRP)-conjugated anti-rabbit IgG (Abcam, cat. #ab6721) or anti-mouse IgG (Cell Signaling technology, cat. #7076) were used as secondary antibodies (1:4000). Bands were visualized with a chemiluminescent HRP substrate (Millipore Sigma, cat. #WBKLS0500). Bands intensities were measured by the Analyze Gels function of the Image J software.

2.7. Cell culture and treatments

HepG2 human hepatocellular carcinoma cells (ATCC, cat. #HB-8065) were cultured in Eagle's Minimum Essential Medium (EMEM) supplemented with fetal bovine serum (10%), penicillin (100 U/mL) and streptomycin (100 μg/mL) under standard conditions (37ºC, 5% CO_2). Cells were then starved 24 h in fetal bovine serum-free EMEM and treated 6 h with 0.25 mM of an equimolar mixture of sodium hexanoate (C8) and sodium decanoate (C10). When required, cells were exposed to either 10 μM T0070907 (PPARγ inhibitor), 10 μM DC260126 (FFAR1/GPR40 antagonist) or DMSO vehicle one hour prior to and during C8/C10 treatment, for a 7 h total exposure time.

2.8. RNA extraction and quantitative PCR

Total RNA was extracted from liver, subcutaneous and epididymal adipose tissues, and HepG2 cells, using TRIzol Reagent (Life Technologies, cat. #15596-018; Carlsbad, USA) following the manufacturer's instructions. One to five μg of total RNA was reverse transcribed into cDNA using SuperScript II reverse transcriptase (Life Technologies, 18064-022, Carlsbad, USA). Quantitative PCR was performed on 50 ng cDNA using gene specific primers pairs (**Table 3**) and the Luna Master Mix reagent (New England Biolabs, cat. # M3003L, USA) in a Light Cycler 480 thermocycler (Roche, cat.# 05015278001). Gene expression was calculated using the comparative ΔCt method (47).

2.9. Statistical analysis

Data are presented as mean ± standard error of the mean. The GraphPad 8 software was used to perform Student's t-tests. A one-tailed unpaired test was applied, except with data normalized to one control where a "one sample" t-test is appropriate. A *p-value* less than 0.05 was taken as indicative of a statistically significant difference between groups.

3. RESULTS

3.1. A high-fat diet enriched in MCT does not adversely affect body weight or insulin sensitivity

Mice of cohort A were three-week old male C57BL/6 fed either the LFD or the three different isocaloric fat-rich diets for 10 weeks (**Fig.1A-B**). A standard high-fat diet (HFD) containing 45% kcal from LCT was used as an obesogenic control diet. The M20 HFD contained 20% kcal from MCT while the M40 HFD contained 40% kcal from MCT.

As expected, HFD feeding resulted in a 33% weight gain relative to LFD feeding (**Fig.1C, Supp.Fig.S1**). Interestingly, stepwise replacement of LCT by MCT (M20 and M40 diets) decreased the impact of HFD on weight gain in a dose-dependent manner. Even more, mice on the M40 diet exhibited a 10% smaller weight gain than the LFD controls (**Fig.1C**, **Supp.Fig.S1**). Energy intake was equivalent among experimental groups (**Fig.1D**) showing that the effects of the M20 and M40 diets were due to their low food efficiency ratio relative to the standard HFD (**Fig.1E**), avoiding the loss of insulin

sensitivity (**Fig.1F**) and glucose clearance efficiency (**Fig.1G, Supp.Fig.S1**). M40-fed mice even exhibited an insulin sensitivity similar to LFD lean controls (**Fig.1F-H, Supp.Fig.S1**). Overall, MCT replacement diminished (M20) or completely prevented (M40) HFD-induced insulin resistance.

3.2. A high-fat diet enriched in MCT improves markers of hepatic health

Since liver steatosis is a well-established comorbidity effect of obesity and insulin resistance (48), we evaluated the impact of our experimental diets on hepatic tissue. Standard HFD induced a strong fat accumulation in livers. This was characterized by lipid macrovesicles reaching 63 μm^2 (*versus* 15 μm^2 in LFD) and covering 22% of the tissue area (*versus* 2.5% in LFD; **Fig.2A-C**). The M20 diet was also steatogenic, but LD were 25% smaller and less abundant in M20-fed livers than after standard HFD feeding (**Fig.2A-C**). Interestingly, the M40 diet had a radical effect, causing a near-abolishment of hepatic LD (**Fig.2A).** Indeed, M40 substantially decreased (3-fold) the average hepatic LD size and tended to decrease (2-fold) the total area covered by LD, relative to LFD control (**Fig.2B,C**). None of the four experimental diets induced collagen fiber infiltration as evidenced by the complete lack of blue stains within livers parenchyma following Masson's trichrome histological preparation (**Fig.2A**). This indicates that hepatic fibrosis was not induced. Consistently with LD content, liver weight was increased by 60% and 50% in HFD-fed and M20-fed mice respectively, compared to LFD (**Fig.2D**). Interestingly, liver weight was decreased in M40-fed mice, being even 20% lower than in LFD-fed mice. The liver index (liver to body weight ratio) remained unchanged among the 4 groups (*data not shown*).

Hepatic steatosis is often associated with insulin resistance and, as a corollary, absence of hepatic steatosis is favorable to insulin sensitivity preservation (49, 50). We therefore measured the phosphorylation state of Akt kinase (on serine 473), a reliable marker of tissue-specific insulin sensitivity (51). This phosphorylation tended to be inhibited in HFD-fed mice compared to LFD-fed mice, while livers of mice fed with the M20 and M40 diets displayed a strong increase in Akt phosphorylation relative to HFD (**Fig.2E**). This suggests that the MCT-containing diets potentiate liver's insulin sensitivity, contrary to steatogenic HFD.

3.3. A high-fat diet enriched in MCT triggers the overexpression of thermogenesis markers in the liver

Given that the M40 HFD diet did not induce an increase in hepatic weight or LD content, we reasoned that a MCT-rich diet might activate specific lipid catabolic processes in the liver. Expression of the lipolysis marker *Atgl* was not overly modulated by the fatty diets (**Fig.3A**) while, relatively to HFD, MCT diets dose-dependently increased the expression of the beta-oxidation and mitochondrial biogenesis markers *Cpt1a* and *Ppargc1a*, respectively (**Fig.3B-C**). Strikingly, the M40 diet triggered a 6.7-fold increase in *Ucp1* gene expression, a key thermogenesis marker, at a level close to statistical significance (p=0.066, **Fig.3D**). To further characterize thermogenesis in liver samples, we measured the abundance of Vdac1 and Ucp1 proteins, as well as the phosphorylation of Ampk (on threonine 172) which reflects the intracellular AMP:ATP balance. The three markers were increased by more than 2-fold, in livers of M40-fed mice (**Fig.3E-G**). The M20 diet did not trigger these thermogenic features.

To delineate the molecular mechanism underlying the induction of *Ucp1* expression by MCT consumption, we evaluated the expression of canonical endogenous activators of thermogenesis. Neither *Adrb3* gene expression (37), PPARγ activity (31) – as reported by the expression of its hepatic target gene *Cd36* – nor *Fgf21* gene expression (52) was increased in livers from M40-fed mice (**Supp.Fig.S2**). We next evaluated the direct effect of MCFA on hepatocytes, as they are abundant (in their non esterified form) in the hepato-portal system after the digestion of dietary MCT (38, 39, 53). This may indeed trigger hepatic *Ucp1* expression trough activation of the above mentioned FFAR1/GPR40. Treatment of HepG2 human hepatoma cells with an equimolar mixture of C8 and C10 (mimicking MCT oil) effectively increased *UCP1* gene overexpression by 3.5-fold (**Fig.3H**). Moreover, this induction was significantly impeded in the presence of a FFAR1/GPR40 inhibitor, confirming the involvement of this receptor (**Fig.3H**). We also confirmed that a PPARγ antagonist has no inhibitory effect on MCFA-induced *UCP1* overexpression (**Fig.3H**).

3.4. A high-fat diet enriched in MCT does not trigger WAT expansion

Mice on M40 displayed a lower level of circulating triglycerides than HFD-fed mice, at a level similar to that of LFD-fed mice (**Fig.4A**). Mice fed with high-fat diets enriched in MCT showed, in a dose-dependent manner, lower circulating leptin levels than mice raised on the standard HFD. Moreover, leptin level was 6 times lower in M40-fed mice than in LFD-fed mice (**Fig.4B**).

These results indicated that the MCT diets potentially lowered white adiposity in comparison with the HFD, because both circulating leptin and triglyceride levels are key markers positively correlated with white adiposity expansion (54, 55). Interestingly, the epididymal fat deposit was almost absent in M40-fed mice (**Fig.4C**). The subcutaneous WAT was also less abundant in M40-fed than in any other mice from the cohort (*data not shown*). While the HFD almost doubled adipocyte size, M20 and M40 MCT-enriched diets dose-dependently prevented adipocyte hypertrophy in both epididymal WAT (**Fig.4D,E**) and subcutaneous WAT (**Fig.5A-B)**. Moreover, the average size of subcutaneous adipocytes tended to be lower in M40-fed mice than in the LFD control (**Fig.5A,B**).

To better understand the underlying molecular mechanisms at play in these adipose tissues, we measured the expression levels of various genes involved in lipid metabolism. In epididymal tissue, the experimental diets did not modulate the expression of the *Srebf1* gene (**Fig.4F**) which encodes for the master upregulator of lipogenesis Sterol regulatory element-binding transcription factor 1 (Srebp1) (56). Feeding mice with the M40 diet increased *Cd36* expression 2-fold (**Fig.4G**), while *Cpt1a* expression was increased 3-fold by the three energy dense diets (**Fig.4H**). *Ppargc1a* expression was inhibited under the HFD and M20 diet, and was maintained to a similar level than for the LFD under the M40 diet (**Fig.4I**). Expression of *Ucp1* was not modulated either (**Fig.4J**). In subcutaneous adipose tissue, dietary MCT replacement dose-dependently decreased *Srebf1* expression and increased *Cd36* expression (4.5-fold under M20 and 3-fold under M40), relative to the HFD (**Fig.5C,D**). Our experimental diets had little or no effect on *Cpt1a* and *Ppargc1a* expression (**Fig.5E,F**). *Ucp1* expression was decreased to residual levels by the HFD and M20 diets but was preserved by the M40 diet (**Fig.5G**). Overall, compared to the standard HFD, dietary MCT had a more benefic impact on lipid metabolism in subcutaneous than in epididymal adipocytes.

3.5. Body weight and insulin resistance are reduced in metabolically unhealthy obese mice raised on a high-fat diet enriched in MCT

Since M40 ameliorates the metabolic features of healthy mice, we hypothesized that a MCT-enriched diet could ameliorate the metabolic disorders observed in unhealthy obese animals. Therefore, we fed C57BL/6 male mice during 10 weeks with the standard HFD in order to induce marked weight gain, high fasting glycemia and glucose intolerance (**Supp.Fig.S3**). We then transferred these mice to LFD, M20 or M40 diets for 10 additional weeks (cohort B; **Fig.6A**). We also maintained one group on the HFD as control. Following the week of diet switch, weight gain continued to increase in the HFD and M20 groups (**Fig.6B,C**). Conversely, following the diet switch, the LFD as well as the M40 triggered a rapid weight loss sustained during six weeks, before a slight increase to the initial values (**Fig.6B**). Despite this late rescue, LFD and M40 globally triggered 2% and 5% weight loss, respectively, in obese mice (**Fig.6C**).

Global energy intake, after the diet switch, was equal among HFD-, M20- and M40-fed mice, and 13% higher than under LFD (**Fig.6D**), maybe resulting from appetizing effect of fats. While HFD and M20 impaired glucose homeostasis, M40 and LFD rescue glucose homeostasis (**Fig.6E,F, Supp.Fig.S4,S5**). However, the M20 diet failed to reverse weight gain (**Fig.6B,C)** or alterations in glucose homeostasis (**Fig.6E,F; Supp.Fig.S4,S5**).

3.6. A high-fat diet enriched in MCT improves steatosis and stimulates the expression of thermogenesis markers in the liver of obese animals

We next characterized the livers of cohort B mice. Switching from HFD to the M40 diet significantly decreased hepatic steatosis, in comparison with replacement by M20 or LFD (**Fig.7A**). Compared to LFD, the M40 diet led to a 2-fold decrease of hepatic LD size, and a near statistically significant ($p=0.54$) 2-fold decrease of hepatic LD tissue area coverage (**Fig.7B,C**). We noticed a heterogenous distribution of LD in liver samples from MCT-fed mice. LD-rich areas were interspersed with regions depleted in LD, and these depleted regions were systematically located around a vessel (**Fig.7A**; *4x zoom*). At the same time, both liver weight and liver index were further increased by HFD and M20

diet, and 15% lower under the M40 diet, compared to LFD-fed mice (**Fig.7D,E**). Consistently with these results, hepatic basal phosphorylation of Akt (S473) was inhibited 2-fold by the HFD and the M20 diet, and preserved by the M40 diet, relative to the LFD (**Fig.7F**).

To evaluate the importance of lipid catabolism in the antisteatogenic effect of dietary MCT, we then measured the hepatic expression of genes related to this process. None of the diets modulated hepatic *Atgl* expression (**Fig.7G**). Relative to LFD, both M20 and M40 diets tended to induce hepatic *Cpt1a* expression (**Fig.7H**). However, only the M40 diet increased *Ppargc1a* and *Ucp1* hepatic expression, by 1.6-fold and 2.5-fold respectively (**Fig.7I,J**).

3.7. Expression of thermogenesis markers are increased in subcutaneous WAT of obese mice on a MCT enriched diet.

Considering that MCT enriched high-fat diets had a stronger impact on subcutaneous adipocytes than on epididymal adipocytes in cohort A, we evaluated the impact of our diet switch on the expression of metabolic markers in the subcutaneous WAT of obese animals from cohort B. Surprisingly, transition from the HFD to the M40 diet increased both *Srebf1* and *Cd36* expression relative to the M20 diet and HFD control (**Fig.8A,B**). Moreover, the M20 diet tends to decrease the expression of *Cpt1a* while the M40 tends to increase it (**Fig.8C**). Interestingly, both the M20 and M40 diets tended, but not significatively, to increase *Ppargc1a* and *Ucp1* thermogenesis markers expression, in a dose-dependent manner (**Fig.8D,E**).

4. DISCUSSION

In this study we characterized the impact of dietary MCT on mouse metabolic health. We showed that replacement of LCT by MCT dose-dependently reduces the obesogenic and steatogenic effect of a HFD. Dietary MCT trigger marked elevation of thermogenesis features at the hepatic level. These thermogenic features are concomitant with a reduction

of liver steatosis, body weight loss, and metabolic improvement in unhealthy obese mice. The most notable results were obtained in the liver, not in adipose tissue, supporting the central role of hepatic thermogenesis in the metabolically beneficial effects of dietary MCT. The main limitation of our study is that only male mice were used. As sexual dimorphism has previously been observed in relation to MCT feeding and lipid metabolism (57), the impact of MCT enriched diets on obesity-related metabolism features in females should be investigated in further studies.

Common sources of saturated and monounsaturated LCT, such as lard, are consensually thought to promote unhealthy lipid accumulation (58, 59). Herein, replacement of lard by MCT in fat-rich diets dose-dependently prevents obesity induction. This result is consistent with the propensity of medium chain lipids towards rapid oxidation (41). Previous studies also reported that MCT-based lipid-rich diets (comparable to the M40 diet) prevent weight gain and obesity features in rodents (41, 60-62). Going further, our study shows that M40 feeding resulted in a body weight gain substantially lower than under LFD feeding. A plausible mechanism explaining this observation is the strong effect of the M40 diet on thermogenic and lipid catabolism features, especially in the liver, a result never documented following removal of lard from diets (63). By triggering thermogenic catabolic processes in the liver, in a manner not induced by LFD, this MCT-rich diet likely promotes the mobilization for oxidation of hepatic, circulating and adipose fat stores, leading to a significant reduction in body mass. This clearly suggests that the effects observed are induced by the addition of MCT and not by the removal of lard. We also showed here that dietary MCT stimulated the hepatic lipid catabolic process, as evidenced by increased *Cpt1a* and *Ppargc1a* gene expression (**Fig.3B,C**). In agreement with our observations, MCT and their unesterified MCFA derivatives have been reported to promote lipid catabolism in isolated hepatocytes (21, 64), in muscles (65, 66), in WAT and BAT (36, 37), as well as mitochondrial biogenesis and activity in piglet livers (67).

We also showed a marked induction of *Ucp1* expression in liver samples of mice fed with the M40 diet. This was surprising since *Ucp1* has been reported to be mainly expressed in BAT and at a lower extent in WAT, but not in liver (68). However, we showed that

hepatic *Ucp1* gene expression in M40-fed mice was accompanied by elevated expression of the mitochondrial abundance marker Vdac1(**Fig.3E**) (69, 70) and the Ucp1 protein (**Fig.3F**). The expression of phosphorylated Ampk (T172) (**Fig.3G**) was also increased indicating a low ATP:ADP+AMP ratio (7). This suggests that hepatic Ucp1 induction, after MCT-enriched feeding, was relevant in terms of functional thermogenesis, a catabolic pathway which promotes fat depletion. Moreover, phosphorylated Ampk directly participates in the activation of lipid catabolism (6, 7), which could in turn contribute to the lack of hepatic steatosis (**Fig.2A-D**) and insulin resistance (**Fig.2E**), following MCT intake. Thermogenesis is known to decrease reactive oxygen species production (35, 71), and may in part contributed to M40-fed mice hepatic health.

Several investigators reported that dietary MCT boost thermogenesis in brown adipose tissues (36, 37, 72) and upregulate thermogenesis markers (such as UCP1) in skeletal muscles (73). In terms of liver effects, Chamma *et al.* recently reported that a MCT enriched diet (similar to our M40 diet) also increased hepatic Pgc1α and Ucp3 expression levels (74). However, this was associated with marked liver steatosis, in contradiction with our results. This discrepancy probably reflects the fact that the MCT-rich diet used by Chamma *et al.* was 30% more caloric than their control diet (74), Moreover, this caloric surplus was not provided by fats or sugar, explaining lack of adiposity, but by casein whose long term consumption at high doses is known to trigger strong liver steatosis (75).

Reproducing the *in vivo* effect of dietary MCT, we showed that MCFA treatment, at physiologically relevant concentrations (76, 77) also significantly increased *UCP1* expression in cultured HepG2 cells (**Fig.3H**). This observation demonstrates that MCFA derived from dietary MCT, known to efficiently enter the hepatic portal vein circulation, have the potential to directly foster thermogenesis of hepatic parenchyma. Our data also suggests that this effect is probably mediated by the FFAR1/GPR40 receptor (**Fig.3H**). Interestingly, C8 and C10 are known FFAR1/GPR40 agonists (78). In addition, treatment of mouse livers and HepG2 cells with the FFAR1/GPR40 agonist GW9508 prevented, in an AMPK-activation dependent manner, lipid accumulation induced by steatogenic challenges (45). In addition, C10 was shown to amplify glucose-stimulated insulin secretion by pancreatic β-cells in a FFAR1/GPR40-dependent fashion (79). Of

note, *UCP1* induction by MCFA was not completely abrogated by the FFAR1/GPR40 antagonist in our assays, suggesting that other pathways may be involved in mediating the MCFA effect on *UCP1* expression.

Our study suggests that high amounts of MCFA derived from hydrolyzed dietary MCT reach the liver, resulting in hepatic LD depletion likely via an FFAR1/GPR40-dependent activation of thermogenesis. Previous reports have shown that medium chain lipids also decrease VLDL production by hepatocytes (80-82). These reports, coupled with our observations, lead us to hypothesize that MCT decrease the availability of circulating fatty acids, thus drastically reducing the fatty acid supply needed for triglyceride synthesis and storage by peripheral tissues such as WAT. Consistently with the metabolic profile observed on our MCT-fed mice, prevention of adipocyte hypertrophy is, furthermore, a well-recognized marker for optimal metabolic health (83). However, MCT-rich diets did not increase thermogenesis markers in WAT, highlighting the importance of hepatic thermogenesis in the metabolic effects of MCT in lean mice.

Even if the liver readily oxidizes most of dietary MCFA, it seems that a small proportion of MCFA, mainly as C10 (84), evades liver catabolism to induce peripheral effects (85). In fact, it has been suggested that, in rats, dietary MCFA exert a direct lowering effect on epididymal and perirenal white adiposity by decreasing *PPARγ* and *CEBPα* gene expression, as well as LPL activity (85). Other studies, conducted on 3T3-L1 preadipocytes, have revealed that C8 and C10 activate PPARγ, promoting adipocyte differentiation (44, 86). In our study, MCT presumably increased PPARγ activity in WAT, as revealed by the induction of its *Cd36* target gene (87). Yet, adipose expansion could not occur for the reason proposed above.

In metabolically unhealthy obese mice, we showed that the M40 diet decreased body weight, insulin resistance and liver steatosis. This result is in agreement with a previous study showing that both C8 and C10 decreased lipid stores within steatosed hepatocytes by promoting lipolysis and decreasing lipogenesis (64). In our obese mice however, hepatic *Atgl* was not increased by MCT feeding, but *Ppargc1a* and *Ucp1* were induced, suggesting that *in vivo* resorption of hepatic steatosis by MCT diets involves thermogenesis rather than lipolysis. Interestingly in cohort B, liver samples of M20-fed

mice were dotted with areas without steatosis around blood vessels (**Fig.7A**). One possibility is that dietary MCFA reach hepatic blood vessels from which they undergo simple diffusion to activate catabolic features in the surrounding parenchyma.

Otherwise, markers of thermogenesis tended to increase in subcutaneous adipose tissue of mice from cohort B on the M40 diet (**Fig.8C-E**). This suggests that, in obese mice, MCT have the potential to trigger the browning of WAT. In accordance with this concept, MCT feeding reduces obesity in part via the elevation of thermogenesis from scapular BAT (37). This may be explained in part by the fact that in obese mice with steatosis, hepatic lipid catabolism is low. Therefore, significant amounts of MCFA (higher than in lean mice) evade liver oxidation, reaching the WAT. Once in the WAT, they could activate PPARγ, triggering the PPAR-dependent browning phenotype (31).

In conclusion, we found that in healthy lean mice, consumption of high amounts of MCT prevent metabolic disorders likely by triggering thermogenesis within the liver, preventing body fat expansion. We suggest that the liver is a key metabolic organ where MCT exert their metabolically beneficial thermogenic effects in a FFAR1/GPR40-dependent manner. In obese metabolically unhealthy mice, MCT-rich diets also improved the metabolic profile, and enhanced the levels of thermogenesis markers in the liver as well as in the subcutaneous WAT. Overall, our study consolidates the concept that dietary MCT are bioactive lipids that could be helpful for the prevention and the treatment of metabolic disorders related to obesity, such as non-alcoholic fatty liver disease, dyslipidemia and insulin resistance.

5. ACKNOWLEDGMENTS AND FINANCIAL SUPPORT

The authors thank Denis Flipo (UQAM) for help with microscopy and image analysis. The authors also acknowledge laboratory interns Sarah-Clohé Lacoste, Nathalie Pesin and Maxime Borret for their technical contribution. The authors are grateful for the feedback provided by Mohamed Amine Lounis (CRCHUM). SAR received doctoral scholarships from FRQNT and *Fondation de l'UQAM*. This research was supported by a

grant from NSERC (Discovery Grants Program). Authors are grateful to SERVIER Medical Art creators for allowing free access to their images bank, which was used to construct the graphical abstract.

6. DISCLOSURES

The authors declare having no conflicts of interest related to this work

7. REFERENCES

1. Bender DA. Introduction to Nutrition and Metabolism, Fifth Edition. Fifth edition ed. Press C, editor2014 23 avr. 2014.
2. Strable MS, Ntambi JM. Genetic control of de novo lipogenesis: role in diet-induced obesity. Crit Rev Biochem Mol Biol. 2010;45(3):199-214.
3. Adeva-Andany MM, Carneiro-Freire N, Seco-Filgueira M, Fernandez-Fernandez C, Mourino-Bayolo D. Mitochondrial beta-oxidation of saturated fatty acids in humans. Mitochondrion. 2019;46:73-90.
4. Calderon-Dominguez M, Mir JF, Fucho R, Weber M, Serra D, Herrero L. Fatty acid metabolism and the basis of brown adipose tissue function. Adipocyte. 2016;5(2):98-118.
5. Frayn KN, Arner P, Yki-Jarvinen H. Fatty acid metabolism in adipose tissue, muscle and liver in health and disease. Essays in biochemistry. 2006;42:89-103.
6. Carlson CA, Kim KH. Regulation of hepatic acetyl coenzyme A carboxylase by phosphorylation and dephosphorylation. The Journal of biological chemistry. 1973;248(1):378-80.
7. Hardie DG. AMP-activated protein kinase: maintaining energy homeostasis at the cellular and whole-body levels. Annu Rev Nutr. 2014;34:31-55.
8. Li Y, Xu S, Mihaylova MM, Zheng B, Hou X, Jiang B, et al. AMPK phosphorylates and inhibits SREBP activity to attenuate hepatic steatosis and atherosclerosis in diet-induced insulin-resistant mice. Cell Metab. 2011;13(4):376-88.

9. Jäger S, Handschin C, St-Pierre J, Spiegelman BM. AMP-activated protein kinase (AMPK) action in skeletal muscle via direct phosphorylation of PGC-1alpha. Proc Natl Acad Sci U S A. 2007;104(29):12017-22.
10. Smith KB, Smith MS. Obesity Statistics. Prim Care. 2016;43(1):121-35, ix.
11. Virtue S, Vidal-Puig A. Adipose tissue expandability, lipotoxicity and the Metabolic Syndrome--an allostatic perspective. Biochim Biophys Acta. 2010;1801(3):338-49.
12. Ebbert JO, Jensen MD. Fat depots, free fatty acids, and dyslipidemia. Nutrients. 2013;5(2):498-508.
13. Chadt A, Scherneck S, Joost H-G, Al-Hasani H. Molecular links between Obesity and Diabetes: "Diabesity": MDText.com, Inc., South Dartmouth (MA); 2000 2000.
14. Al-Dayyat HaM, Rayyan YM, Tayyem RF. Non-alcoholic fatty liver disease and associated dietary and lifestyle risk factors. Diabetes & Metabolic Syndrome: Clinical Research & Reviews. 2018;12(4):569-75.
15. Byrne CD. Ectopic fat, insulin resistance and non-alcoholic fatty liver disease. Proc Nutr Soc. 2013;72(4):412-9.
16. Dietrich P, Hellerbrand C. Non-alcoholic fatty liver disease, obesity and the metabolic syndrome. Best practice & research Clinical gastroenterology. 2014;28(4):637-53.
17. Dostálová J, Hanzl ÍK P, Réblová Z, PokornÝ JAN. Oxidative Changes of Vegetable Oils during Microwave Heating2005.
18. Vingering N, Oseredczuk M, du Chaffaut L, Ireland J, Ledoux M. Fatty acid composition of commercial vegetable oils from the French market analysed using a long highly polar column. OCL. 2010;17(3):185-92.
19. Fischer IP, Irmler M, Meyer CW, Sachs SJ, Neff F, Hrabě de Angelis M, et al. A history of obesity leaves an inflammatory fingerprint in liver and adipose tissue. Int J Obes (Lond). 2018;42(3):507-17.
20. Gao M, Ma Y, Liu D. High-Fat Diet-Induced Adiposity, Adipose Inflammation, Hepatic Steatosis and Hyperinsulinemia in Outbred CD-1 Mice. PloS one. 2015;10(3):e0119784.
21. Rial SA, Ravaut G, Malaret TB, Bergeron KF, Mounier C. Hexanoic, Octanoic and Decanoic Acids Promote Basal and Insulin-Induced Phosphorylation of the Akt-mTOR Axis and a Balanced Lipid Metabolism in the HepG2 Hepatoma Cell Line. Molecules. 2018;23(9).
22. Li Z, Lai ZW, Christiano R, Gazos-Lopes F, Walther TC, Farese RV, Jr. Global Analyses of Selective Insulin Resistance in Hepatocytes Caused by Palmitate Lipotoxicity. Molecular & cellular proteomics : MCP. 2018;17(5):836-49.
23. Tang Z, Zhang W, Wan C, Xu G, Nie X, Zhu X, et al. TRAM1 protect HepG2 cells from palmitate induced insulin resistance through ER stress-JNK pathway. Biochem Biophys Res Commun. 2015;457(4):578-84.
24. Gao D, Nong S, Huang X, Lu Y, Zhao H, Lin Y, et al. The effects of palmitate on hepatic insulin resistance are mediated by NADPH Oxidase 3-derived reactive oxygen species through JNK and p38MAPK pathways. The Journal of biological chemistry. 2010;285(39):29965-73.

25. Zhao N-Q, Li X-Y, Wang L, Feng Z-L, Li X-F, Wen Y-F, et al. Palmitate induces fat accumulation by activating C/EBPβ-mediated G0S2 expression in HepG2 cells. World Journal of Gastroenterology. 2017;23(43):7705-15.
26. Xiao X, Li H, Qi X, Wang Y, Xu C, Liu G, et al. Zinc alpha2 glycoprotein alleviates palmitic acid-induced intracellular lipid accumulation in hepatocytes. Molecular and cellular endocrinology. 2017;439:155-64.
27. Cui XB, Chen SY. White adipose tissue browning and obesity. J Biomed Res. 2016;31(1):1-2.
28. Marinovic MP, Campeiro JD, Lima SC, Rocha AL, Nering MB, Oliveira EB, et al. Crotamine induces browning of adipose tissue and increases energy expenditure in mice. Sci Rep. 2018;8(1):5057.
29. Velickovic K, Wayne D, Leija HAL, Bloor I, Morris DE, Law J, et al. Caffeine exposure induces browning features in adipose tissue in vitro and in vivo. Scientific Reports. 2019;9(1):9104.
30. Nirengi S, Homma T, Inoue N, Sato H, Yoneshiro T, Matsushita M, et al. Assessment of human brown adipose tissue density during daily ingestion of thermogenic capsinoids using near-infrared time-resolved spectroscopy. Journal of biomedical optics. 2016;21(9):091305.
31. Ohno H, Shinoda K, Spiegelman BM, Kajimura S. PPARgamma agonists induce a white-to-brown fat conversion through stabilization of PRDM16 protein. Cell Metab. 2012;15(3):395-404.
32. Zhang Y, Liu Q, Yu J, Yu S, Wang J, Qiang L, et al. Locally Induced Adipose Tissue Browning by Microneedle Patch for Obesity Treatment. ACS Nano. 2017;11(9):9223-30.
33. Betz MJ, Enerback S. Human Brown Adipose Tissue: What We Have Learned So Far. Diabetes. 2015;64(7):2352-60.
34. Fuller-Jackson JP, Henry BA. Adipose and skeletal muscle thermogenesis: studies from large animals. The Journal of endocrinology. 2018;237(3):R99-r115.
35. Brondani LA, Assmann TS, Duarte GC, Gross JL, Canani LH, Crispim D. The role of the uncoupling protein 1 (UCP1) on the development of obesity and type 2 diabetes mellitus. Arquivos brasileiros de endocrinologia e metabologia. 2012;56(4):215-25.
36. Kim H, Choe JH, Choi JH, Kim HJ, Park SH, Lee MW, et al. Medium-Chain Enriched Diacylglycerol (MCE-DAG) Oil Decreases Body Fat Mass in Mice by Increasing Lipolysis and Thermogenesis in Adipose Tissue. Lipids. 2017;52(8):665-73.
37. Zhang Y, Xu Q, Liu YH, Zhang XS, Wang J, Yu XM, et al. Medium-Chain Triglyceride Activated Brown Adipose Tissue and Induced Reduction of Fat Mass in C57BL/6J Mice Fed High-fat Diet. Biomed Environ Sci. 2015;28(2):97-104.
38. Babayan VK. Medium chain triglycerides and structured lipids. Lipids. 1987;22(6):417-20.
39. Bach AC, Babayan VK. Medium-chain triglycerides: an update. Am J Clin Nutr. 1982;36(5):950-62.
40. Eyres L, Eyres MF, Chisholm A, Brown RC. Coconut oil consumption and cardiovascular risk factors in humans. Nutr Rev. 2016;74(4):267-80.

41. Rial SA, Karelis AD, Bergeron KF, Mounier C. Gut Microbiota and Metabolic Health: The Potential Beneficial Effects of a Medium Chain Triglyceride Diet in Obese Individuals. Nutrients. 2016;8(5).
42. Papamandjaris AA, MacDougall DE, Jones PJ. Medium chain fatty acid metabolism and energy expenditure: obesity treatment implications. Life sciences. 1998;62(14):1203-15.
43. Schönfeld P, Wojtczak L. Short- and medium-chain fatty acids in energy metabolism: the cellular perspective. Journal of lipid research. 2016;57(6):943-54.
44. Liberato MV, Nascimento AS, Ayers SD, Lin JZ, Cvoro A, Silveira RL, et al. Medium chain fatty acids are selective peroxisome proliferator activated receptor (PPAR) gamma activators and pan-PPAR partial agonists. PLoS One. 2012;7(5):e36297.
45. Li M, Meng X, Xu J, Huang X, Li H, Li G, et al. GPR40 agonist ameliorates liver X receptor-induced lipid accumulation in liver by activating AMPK pathway. Sci Rep. 2016;6:25237-.
46. Bradford MM. A rapid and sensitive method for the quantitation of microgram quantities of protein utilizing the principle of protein-dye binding. Analytical biochemistry. 1976;72:248-54.
47. Livak KJ, Schmittgen TD. Analysis of relative gene expression data using real-time quantitative PCR and the 2(-Delta Delta C(T)) Method. Methods (San Diego, Calif). 2001;25(4):402-8.
48. Kitade H, Chen G, Ni Y, Ota T. Nonalcoholic Fatty Liver Disease and Insulin Resistance: New Insights and Potential New Treatments. Nutrients. 2017;9(4):387.
49. Salgado AL, Carvalho L, Oliveira AC, Santos VN, Vieira JG, Parise ER. Insulin resistance index (HOMA-IR) in the differentiation of patients with non-alcoholic fatty liver disease and healthy individuals. Arquivos de gastroenterologia. 2010;47(2):165-9.
50. Dentin R, Benhamed F, Hainault I, Fauveau V, Foufelle F, Dyck JR, et al. Liver-specific inhibition of ChREBP improves hepatic steatosis and insulin resistance in ob/ob mice. Diabetes. 2006;55(8):2159-70.
51. Huang X, Liu G, Guo J, Su Z. The PI3K/AKT pathway in obesity and type 2 diabetes. Int J Biol Sci. 2018;14(11):1483-96.
52. Fisher FM, Kleiner S, Douris N, Fox EC, Mepani RJ, Verdeguer F, et al. FGF21 regulates PGC-1alpha and browning of white adipose tissues in adaptive thermogenesis. Genes Dev. 2012;26(3):271-81.
53. Guillot E, Vaugelade P, Lemarchal P, Rerat A. Intestinal absorption and liver uptake of medium-chain fatty acids in non-anaesthetized pigs. The British journal of nutrition. 1993;69(2):431-42.
54. Skurk T, Alberti-Huber C, Herder C, Hauner H. Relationship between adipocyte size and adipokine expression and secretion. The Journal of clinical endocrinology and metabolism. 2007;92(3):1023-33.
55. Ludgero-Correia A, Aguila MB, Mandarim-de-Lacerda CA, Faria TS. Effects of high-fat diet on plasma lipids, adiposity, and inflammatory markers in ovariectomized C57BL/6 mice. Nutrition (Burbank, Los Angeles County, Calif). 2012;28(3):316-23.
56. Wang Y, Viscarra J, Kim SJ, Sul HS. Transcriptional regulation of hepatic lipogenesis. Nat Rev Mol Cell Biol. 2015;16(11):678-89.

57. Tucci S, Flogel U, Spiekerkoetter U. Sexual dimorphism of lipid metabolism in very long-chain acyl-CoA dehydrogenase deficient (VLCAD-/-) mice in response to medium-chain triglycerides (MCT). Biochim Biophys Acta. 2015;1852(7):1442-50.
58. Kim E, Kim EJ, Seo SW, Hur CG, McGregor RA, Choi MS. Meta-review of protein network regulating obesity between validated obesity candidate genes in the white adipose tissue of high-fat diet-induced obese C57BL/6J mice. Crit Rev Food Sci Nutr. 2014;54(7):910-23.
59. Sun D, Zhang L, Chen H, Feng R, Cao P, Liu Y. Effects of Antarctic krill oil on lipid and glucose metabolism in C57BL/6J mice fed with high fat diet. Lipids in health and disease. 2017;16(1):218.
60. Zhou S, Wang Y, Jiang Y, Zhang Z, Sun X, Yu LL. Dietary Intake of Structured Lipids with Different Contents of Medium-Chain Fatty Acids on Obesity Prevention in C57BL/6J Mice. J Food Sci. 2017;82(8):1968-77.
61. Geng S, Zhu W, Xie C, Li X, Wu J, Liang Z, et al. Medium-chain triglyceride ameliorates insulin resistance and inflammation in high fat diet-induced obese mice. Eur J Nutr. 2016;55(3):931-40.
62. De Vogel-van den Bosch J, van den Berg SA, Bijland S, Voshol PJ, Havekes LM, Romijn HA, et al. High-fat diets rich in medium- versus long-chain fatty acids induce distinct patterns of tissue specific insulin resistance. J Nutr Biochem. 2011;22(4):366-71.
63. Luijten IHN, Feldmann HM, von Essen G, Cannon B, Nedergaard J. In the absence of UCP1-mediated diet-induced thermogenesis, obesity is augmented even in the obesity-resistant 129S mouse strain. American Journal of Physiology-Endocrinology and Metabolism. 2019;316(5):E729-E40.
64. Wang B, Fu J, Li L, Gong D, Wen X, Yu P, et al. Medium-chain fatty acid reduces lipid accumulation by regulating expression of lipid-sensing genes in human liver cells with steatosis. Int J Food Sci Nutr. 2016;67(3):288-97.
65. Montgomery MK, Osborne B, Brown SH, Small L, Mitchell TW, Cooney GJ, et al. Contrasting metabolic effects of medium- versus long-chain fatty acids in skeletal muscle. Journal of lipid research. 2013;54(12):3322-33.
66. Wang Y, Liu Z, Han Y, Xu J, Huang W, Li Z. Medium Chain Triglycerides enhances exercise endurance through the increased mitochondrial biogenesis and metabolism. PLoS One. 2018;13(2):e0191182.
67. Zhang H, Li Y, Hou X, Zhang L, Wang T. Medium-chain TAG improve energy metabolism and mitochondrial biogenesis in the liver of intra-uterine growth-retarded and normal-birth-weight weanling piglets. Br J Nutr. 2016;115(9):1521-30.
68. Shore AM, Karamitri A, Kemp P, Speakman JR, Graham NS, Lomax MA. Cold-induced changes in gene expression in brown adipose tissue, white adipose tissue and liver. PloS one. 2013;8(7):e68933.
69. Mazure NM. News about VDAC1 in Hypoxia. Front Oncol. 2016;6:193-.
70. Yeo D, Kang C, Gomez-Cabrera MC, Vina J, Ji LL. Intensified mitophagy in skeletal muscle with aging is downregulated by PGC-1alpha overexpression in vivo. Free Radic Biol Med. 2019;130:361-8.
71. Cadenas S. Mitochondrial uncoupling, ROS generation and cardioprotection. Biochimica et biophysica acta Bioenergetics. 2018;1859(9):940-50.

72. Baba N, Bracco EF, Hashim SA. Role of brown adipose tissue in thermogenesis induced by overfeeding a diet containing medium chain triglyceride. Lipids. 1987;22(6):442-4.
73. Wang Y, Liu Z, Han Y, Xu J, Huang W, Li Z. Medium Chain Triglycerides enhances exercise endurance through the increased mitochondrial biogenesis and metabolism. PloS one. 2018;13(2):e0191182-e.
74. Chamma CM, Bargut TC, Mandarim-de-Lacerda CA, Aguila MB. A rich medium-chain triacylglycerol diet benefits adiposity but has adverse effects on the markers of hepatic lipogenesis and beta-oxidation. Food Funct. 2017;8(2):778-87.
75. Diaz-Rua R, Keijer J, Palou A, van Schothorst EM, Oliver P. Long-term intake of a high-protein diet increases liver triacylglycerol deposition pathways and hepatic signs of injury in rats. The Journal of nutritional biochemistry. 2017;46:39-48.
76. Haidukewych D, Forsythe WI, Sills M. Monitoring octanoic and decanoic acids in plasma from children with intractable epilepsy treated with medium-chain triglyceride diet. Clinical chemistry. 1982;28(4 Pt 1):642-5.
77. Sills MA, Forsythe WI, Haidukewych D. Role of octanoic and decanoic acids in the control of seizures. Archives of disease in childhood. 1986;61(12):1173-7.
78. Huang H, Dai MH, Tao YX. Physiology and therapeutics of the free fatty acid receptor GPR40. Prog Mol Biol Transl Sci. 2014;121:67-94.
79. Pujol JB, Christinat N, Ratinaud Y, Savoia C, Mitchell SE, Dioum EHM. Coordination of GPR40 and Ketogenesis Signaling by Medium Chain Fatty Acids Regulates Beta Cell Function. Nutrients. 2018;10(4).
80. Sato K, Cho Y, Tachibana S, Chiba T, Schneider WJ, Akiba Y. Impairment of VLDL secretion by medium-chain fatty acids in chicken primary hepatocytes is affected by the chain length. The Journal of nutrition. 2005;135(7):1636-41.
81. Tachibana S, Sato K, Cho Y, Chiba T, Schneider WJ, Akiba Y. Octanoate reduces very low-density lipoprotein secretion by decreasing the synthesis of apolipoprotein B in primary cultures of chicken hepatocytes. Biochim Biophys Acta. 2005;1737(1):36-43.
82. Tachibana S, Sato K, Takahashi T, Akiba Y. Octanoate inhibits very low-density lipoprotein secretion in primary cultures of chicken hepatocytes. Comparative biochemistry and physiology Part A, Molecular & integrative physiology. 2002;132(3):621-7.
83. Ghaben AL, Scherer PE. Adipogenesis and metabolic health. Nat Rev Mol Cell Biol. 2019;20(4):242-58.
84. You YQ, Ling PR, Qu JZ, Bistrian BR. Effects of medium-chain triglycerides, long-chain triglycerides, or 2-monododecanoin on fatty acid composition in the portal vein, intestinal lymph, and systemic circulation in rats. JPEN Journal of parenteral and enteral nutrition. 2008;32(2):169-75.
85. Han J, Hamilton JA, Kirkland JL, Corkey BE, Guo W. Medium-chain oil reduces fat mass and down-regulates expression of adipogenic genes in rats. Obesity research. 2003;11(6):734-44.
86. Yang JY, Della-Fera MA, Rayalam S, Park HJ, Ambati S, Hausman DB, et al. Regulation of adipogenesis by medium-chain fatty acids in the absence of hormonal cocktail. J Nutr Biochem. 2009;20(7):537-43.
87. Wheeler MC, Gekakis N. Hsp90 modulates PPARgamma activity in a mouse model of nonalcoholic fatty liver disease. J Lipid Res. 2014;55(8):1702-10.

8. TABLES

Table 1. Caloric breakdown and nutritional composition of diets

Diets	LFD		HFD		M20		M40	
Composition (%)	**g**	**kcal**	**g**	**kcal**	**g**	**kcal**	**g**	**kcal**
Proteins	19,2	20	24	20	24	20	24	20
carbohydrates	67,3	70	41	35	41	35	41	35
fat	4,3	10	24	45	24	45	24	45
total		100		100		100		100
kcal/g	3,85		4,7		4,7		4,7	
Compounds	**g**	**kcal**	**g**	**kcal**	**g**	**kcal**	**g**	**kcal**
Casein, 80 Mesh	200	800	200	800	200	800	200	800
L-cystine	3	12	3	12	3	12	3	12
corn starch	452,2	1808	72,8	291	72,8	291	72,8	291
Maltodextrine	75	300	100	400	100	400	100	400
Sucrose	172,8	691	172,8	691	172,8	691	172,8	691
Cellulose	50	0	50	0	50	0	50	0
Soy oil	25	225	25	225	25	225	25	225
Lard	20	180	177,5	1598	87,4	787	0	0
MCT	0	0	0	0	90,1	811	177,5	1598
minerals	45	0	45	0	45	0	45	0
Vitamins	12	40	12	40	12	40	12	40
TOTAL	**1055**	**4057**	**858,2**	**4057**	**858,2**	**4057**	**858,2**	**4057**

Table 2. Primers sequences for mouse and human genes used in real-time PCR

Species	Gene target	Forward Primer (5′-3′)	Reverse Primer (5′-3′)
Mus musculus	*Atgl*	GGAACATCTCATTCGCTGGC	CCAGGTTGAAGGAGGGATGC
	Cpt1a	GACTCCGCTCGCTCATTCC	ACCAGTGATGATGCCATTCTTG
	Ppargc1a	GTTCACTCTCAGTAAGGGGC	GTCGCTACACCACTTCAATCC
	Ucp1	AACACTTTGGAAAGGGACGAC	CAAAACCCGGCAACAAGAGC
	Srebf1	GGACACTGAGAGACCCCTGC	TCCATTGCTGGTACCGTGAG
	Cd36	GATGACGTGGCAAAGAACAG	TCCTCGGGGTCCTGAGTTAT
	Adrb3	CCTTCAACCCGGTCATCTACTG	CGCACCTTCATAGCCATCAAAC
	Fgf21	ACCGCAGTCCAGAAAGTCTC	TGCAGGCCTCAGGATCAAAG
	Hprt1	TCAGTCAACGGGGGACATAAA	GGGGCTGTACTGCTTAACCAG
Homo Sapiens	*UCP1*	CAACAGCTATGTCCTCCCCG	ACGTTCCAGGATCCAAGTCG
	HPRT1	CCTGGCGTCGTGATTAGTGAT	AGACGTTCAGTCCTGTCCATAA

Table 3. Antibodies used for Western blots

Antibody target	Manufacturer	Catalog number	Source	Concentration Used
p-Akt (S473)	Cell Signaling Technology	4060S	Rabbit	1:2.000
Vdac1	Abcam	ab14734	Mouse	1:1.000
Ucp1	Abcam	ab155117	Rabbit	1:2.000
p-Ampk (T172)	Cell Signaling Technology	2535S	Rabbit	1:2.000
Cyclophilin-B	Abcam	ab16045	Rabbit	1:50.000
α-Tubulin	Abcam	ab4074	Rabbit	1:50.000

9. FIGURE LEGENDS

Figure 1. High-fat diets enriched in MCT do not adversely affect body weight nor insulin sensitivity. (**A**) Experimental timeline for cohort A. Mice were raised for 10 weeks on diets LFD, HFD, M20 and M40. (**B**) Percentage of energy content (kcal) from long chain triglycerides (LCT) and medium chain triglycerides (MCT) in the four diets. The dashed line shows the standard 45% kcal content from fat. (**C**,**D**,**E**) Area under curve (AUC) of body weight gain, total energy intake, and food efficiency ratio during 10 weeks of diets, for each group (n = 8). (**F**) HOMA-IR determined for each diet group at week 10 (n = 4). (**G**,**H**) AUC of glycaemia variations measured during glucose tolerance tests (GTT) at week 8, and insulin tolerance tests (ITT) at week 9 (n = 4). Data are shown as mean ± SEM. Asterisks (*) are used to indicate statistical comparisons with the LFD group while number signs (#) denote comparisons with the HFD control. Student's t-test: * $p < 0.05$, ** $p < 0.01$, *** $p < 0.001$.

Figure 2. A high-fat diet rich in MCT improves markers of hepatic health. (**A**) Representative images of liver sections from cohort A animals, stained with Masson's trichrome. Blue arrows point to examples of very small and sporadic LD in M40 hepatic samples. Scale bar: 200 microns. (**B**,**C**) Quantification of lipid droplet size and proportion of tissue area occupied by lipid droplets in the liver sections (n = 3). (**D**) Liver weight (n = 8). (**E**) Phosphorylation level of AKT (on Ser473) in liver homogenates (n = 8). Representative Western blots are shown. Phospho-AKT expression was normalized to Cyclophilin-B. Data are shown as mean ± SEM. * compare with the LFD group. # compare with the HFD control. Student's t-test: * $p < 0.05$, ** $p < 0.01$, *** $p < 0.001$.

Figure 3. A high-fat diet rich in MCT triggers the overexpression of key markers of thermogenesis in liver. (**A-D**) Gene expression of *Atgl*, *Cpt1a*, *Ppargc1a* (n = 4) and *Ucp1* (n = 7) normalized by *Hprt1*, in hepatic tissue from cohort A. (**E-G**) Protein expression of Vdac1, Ucp1 and phospho-Ampk (on Thr172) in hepatic tissue (n = 8). Representative Western blots are shown. Vdac1 was normalized to α-Tubulin while Ucp1 and phospho-Ampk were normalized to Cyclophilin-B. (**H**) Expression of *UCP1*

transcript in HepG2 cells, normalized to the *Hprt1* (n = 3). Cells were treated 6h with MCFA (125 µM C8 + 125 µM C10) and with either vehicle (CTL), the PPARγ inhibitor T0070907 (PPARγI, 10µM) or the FFAR1/GPR40 antagonist inhibitor DC260126 (GPR40I, 10µM). *Ucp1* expression were normalized to vehicle-treated cells. Data are shown as mean ± SEM. * compare with the LFD group and # compare with the HFD group. & designate comparisons with the DMSO-treated cells., and † compare with the MCFA-treated condition. Student's t-test: * $p < 0.05$, ** $p < 0.01$, *** $p < 0.001$, **** $p < 0.0001$.

Figure 4. A high-fat diet rich in MCT exert beneficial effects on visceral white adipose tissue. (**A**,**B**) Circulating triglycerides (TG) and leptin from cohort A plasma samples (n = 4). (**C**) Representative photographs of dissected mouse abdomens with epididymal (Ep) WAT highlighted in yellow. (**D**) Representative images of epididymal white adipose tissue sections, stained with H&E. (**E**) Quantification of adipocyte size in the tissue sections (n = 3). (**F-J**) Expression of *Srebf1*, *Cd36*, *Cpt1a*, *Ppargc1a* and *Ucp1* transcripts, normalized to *Hprt1*, in epididymal white adipose tissue (n = 4). Data are shown as mean ± SEM. * compare with the LFD group, and # compare with the HFD group. Student's t-test: * $p < 0.05$, ** $p < 0.01$, *** $p < 0.001$, **** $p < 0.0001$.

Figure 5. A high-fat diet enriched in MCT exert beneficial effects on subcutaneous white adipose tissue. (**A**) Representative images of subcutaneous white adipose tissue (WAT) tissue sections, stained with H&E. (**B**) Quantification of adipocyte size in the tissue sections (n = 3). (**C-G**) Expression of *Srebf1*, *Cd36*, *Cpt1a*, *Ppargc1a* and *Ucp1* transcripts, normalized to *Hprt1* (n = 4). Data are shown as mean ± SEM. * compare with the LFD group, and # compare with the HFD control. Student's t-test: * $p < 0.05$, ** $p < 0.01$, *** $p < 0.001$.

Figure 6. Body weight and insulin resistance are reduced in metabolically unhealthy obese mice fed a high-fat diet enriched in MCT. (**A**) Experimental timeline for cohort B. Mice were raised for 10 weeks on HFD then switched to diets LFD, HFD, M20 and M40 for another 10 weeks. (**B**) Body weight change after diet switch in percentage *versus*

body weight measured at week 10 (n=8). The dotted line represents a theorical unchanged body weight percentage. (**C**) Area under curve (AUC) of body weight change after diet switch, in comparison with AUC of the theorical unchanged (Stable, hatched histogram) body weight percentage (n = 8). (**D**) AUC of total energy intake measured for each group from the day of diet switch (n=2). (**E,F**) AUC of GTT and ITT results measured before (at week 8 and week 9 respectively) and after diet switch (n = 4). The dotted lines outline the values before diet switch. Data are shown as mean ± SEM. * compare with the LFD group. Ψ is used for comparisons of body weight change percentage with theorical unchanged (**B**), and $ for comparisons with the pre-switch diet values (**C,D**). Student's t-test: * $p < 0.05$, ** $p < 0.01$, **** $p < 0.0001$.

Figure 7. A high-fat diet enriched in MCT improves steatosis modulating hepatic lipid catabolism in obese animals. (**A**) Representative images of liver sections from cohort B animals, stained with Masson's trichrome. Yellow arrowheads point to blood vessels. Zoom boxes show a 4-fold magnification of regions of the microscope field. (**B**,**C**) Quantification of LD size and proportion of tissue area occupied by LD in the liver sections (n = 3). (**D**,**E**) Liver weight and liver index (liver weight / body mass) in cohort B (n = 8). (**F**) Evaluation of phospho-AKT (Ser473) by Western blot normalized to Cyclophilin-B in liver homogenates (n = 8). Representative blots are shown. Gene expression of hepatic *Atgl, Cpt1a*, *Ppargc1a* and *Ucp1*, normalized to *Hprt1* (n = 4). Data are shown as mean ± SEM. * compare with the LFD group, and # compare with the HFD group. Student's t-test: * $p < 0.05$, ** $p < 0.01$, **** $p < 0.0001$.

Figure 8. Expression of thermogenesis markers are increased in subcutaneous WAT of obese mice on a MCT enriched diet. (**A-E**) Gene expression of *Srebf1*, *Cd36*, *Cpt1a*, *Ppargc1a*, and *Ucp1* normalized to *Hprt1*, in subcutaneous WAT from cohort B (n = 4). Data are shown as mean ± SEM. * compare with the LFD group, and # compare with the HFD group. Student's t-test: * $p < 0.05$, ** $p < 0.01$.

Supplementary Figure 1. High-fat diets rich in MCT do not adversely affect body weight nor insulin sensitivity, in cohort A. (**A**) Body weight change in percentage of body weight measured at week 0 (n=8). (**B**) Glucose tolerance test (GTT) and (**C**) insulin tolerance test (ITT) respectively performed at weeks 8 and 9 (n=8). Data are shown as mean ± SEM. * compare with the LFD group, and # compare with the HFD group corresponding to the same time on x-axis. Student's t-test: * $p < 0.05$, ** $p < 0.01$, **** $p < 0.0001$.

Supplementary Figure 2. Hepatic markers of canonical thermogenesis-activating pathways are not induced by MCT-rich diets, in cohort A mice. (**A-C**) Expression of *Adrb3*, *Cd36*, and *Fgf21* transcripts, normalized to *Hprt1*, in liver samples from cohort A (n = 4). Data are shown as mean ± SEM. * compare with the LFD group, and # compare with the HFD group. Student's t-test: * $p < 0.05$.

Supplementary Figure 3. High fat diet (HFD)-induced obesity and glucose homeostasis impairment in mice of cohort B. (**A**) body weight (n=32), (**B**) fasting glycemia (n=4) and (**C**) AUC of GTT (n=4) measured at early and late timepoints of the 10-weeks long HFD-based protocol feeding for mice of cohort B. Data are shown as mean ± SEM. * compare with week 0 (**A,C**) or week 3 (**B**), and # compare with week 8 (**A,B**). Paired student's t-test: ** $p < 0.01$, **** $p < 0.0001$.

Supplementary Figure 4. Glucose intolerance is reduced in metabolically unhealthy obese mice fed a high-fat diet rich in MCT. GTT performed on mice from cohort B at weeks 0 and 8 of the obesity-induction step, then at week 8 after the diet switch. Data were obtained from mice that have been transferred to LFD (**A**), HFD (**B**), M20 (**C**) and M40 (**D**) diets (n=4). Results are mean ± SEM. * compare each timepoint of the GTT measured at week 8 with the equivalent timepoint measured at week 0, and # similarly compare week 18 with week 8. Paired student's t-test: * $p < 0.05$, *** $p < 0.001$, **** $p < 0.0001$.

Supplementary Figure 5. Insulin resistance is reduced in metabolically unhealthy obese mice fed a high-fat diet rich in MCT. ITT performed on mice from cohort B at week 9 of the obesity-induction step, then at week 9 after the diet switch. Data were obtained from mice that have been transferred to LFD (**A**), HFD (**B**), M20 (**C**) and M40 (**D**) diets (n=4). Results are mean ± SEM. # compare each timepoint of the ITT measured at week 19 with the equivalent timepoint measured at week 9. Paired student's t-test: # $p < 0.05$, ## $p < 0.01$, ### $p < 0.001$.

Figure 1

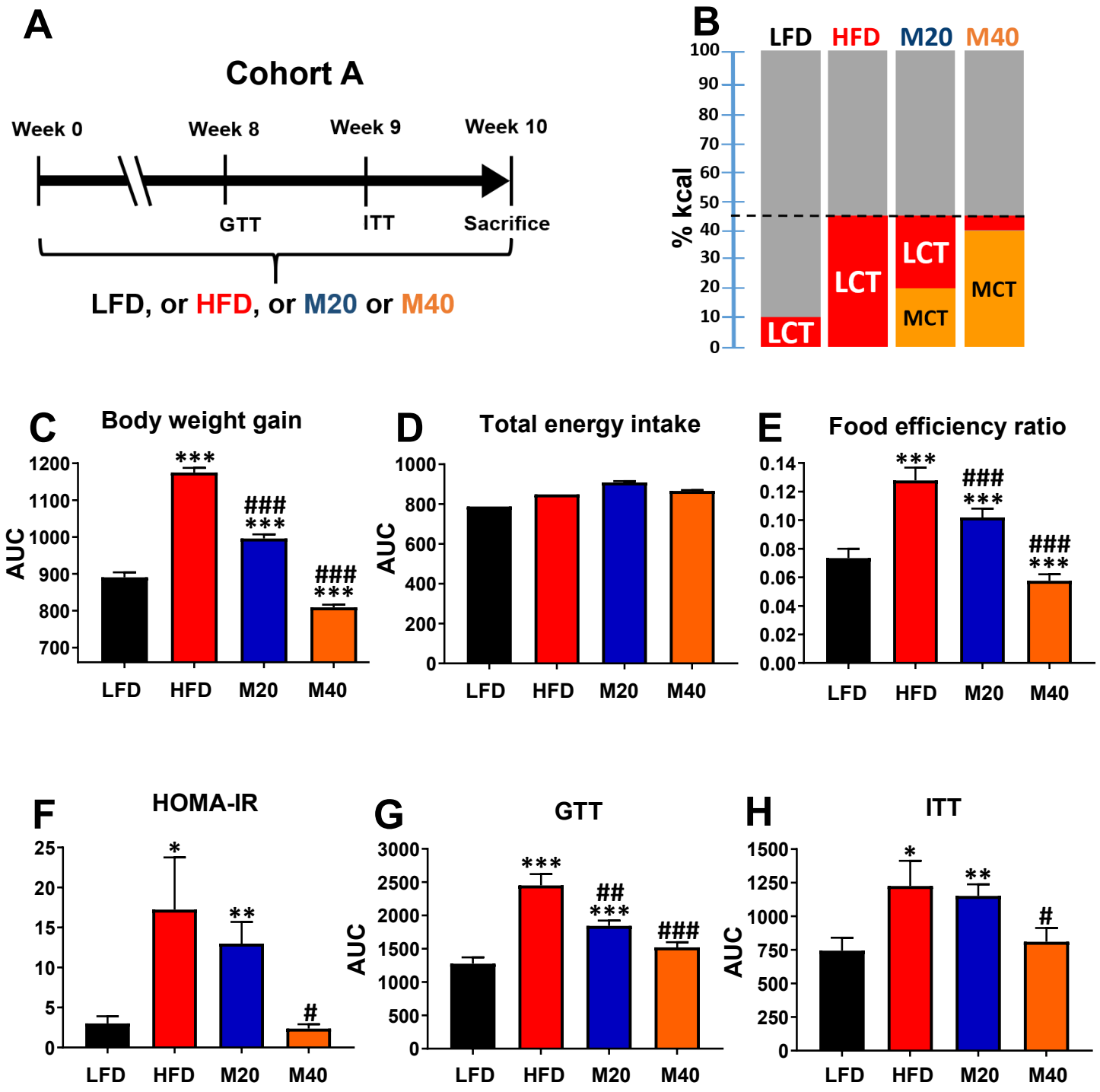
A
Cohort A
Week 0
Week 8
Week 9
Week 10
GTT
ITT
Sacrifice
LFD, or HFD, or M20 or M40
B
LFD
HFD
M20
M40
% kcal
LCT
LCT
LCT
MCT
MCT
C
Body weight gain
AUC
D
Total energy intake
AUC
E
Food efficiency ratio
F
HOMA-IR
G
GTT
AUC
H
ITT
AUC

Figure 2

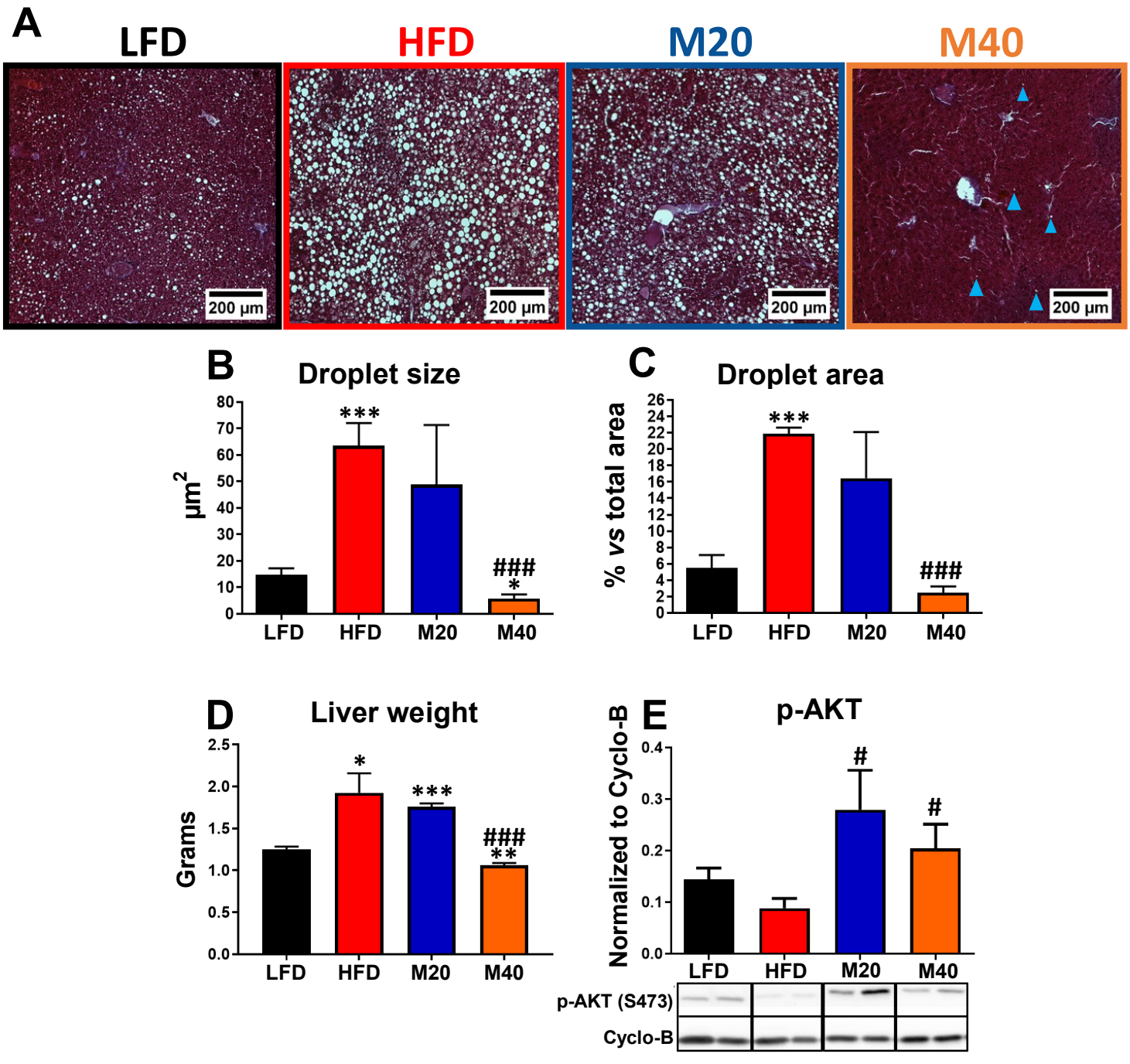
A
LFD
HFD
M20
M40
200 µm
B
Droplet size
µm2
***
###
*
C
Droplet area
% vs total area
***
###
D
Liver weight
Grams
*
***
###
**
E
p-AKT
Normalized to Cyclo-B
#
#
p-AKT (S473)
Cyclo-B

Figure 3

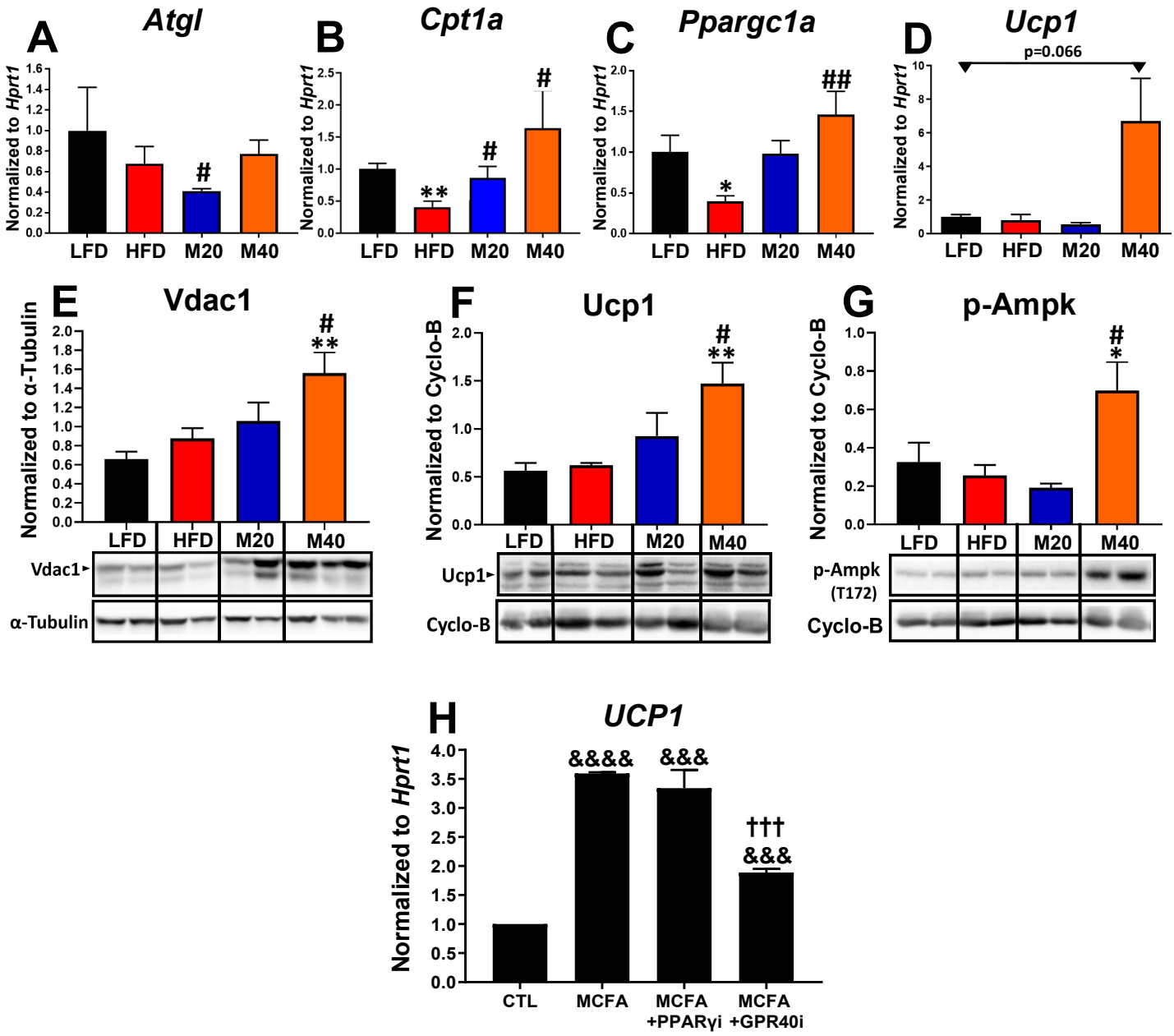
A
Atgl
Normalized to Hprt1
LFD HFD M20 M40
B
Cpt1a
Normalized to Hprt1
LFD HFD M20 M40
C
Ppargc1a
Normalized to Hprt1
LFD HFD M20 M40
D
Ucp1
p=0.066
Normalized to Hprt1
LFD HFD M20 M40
E
Vdac1
Normalized to α-Tubulin
LFD HFD M20 M40
Vdac1
α-Tubulin
F
Ucp1
Normalized to Cyclo-B
LFD HFD M20 M40
Ucp1
Cyclo-B
G
p-Ampk
Normalized to Cyclo-B
LFD HFD M20 M40
p-Ampk (T172)
Cyclo-B
H
UCP1
Normalized to Hprt1
CTL
MCFA
MCFA +PPARγi
MCFA +GPR40i

Figure 4

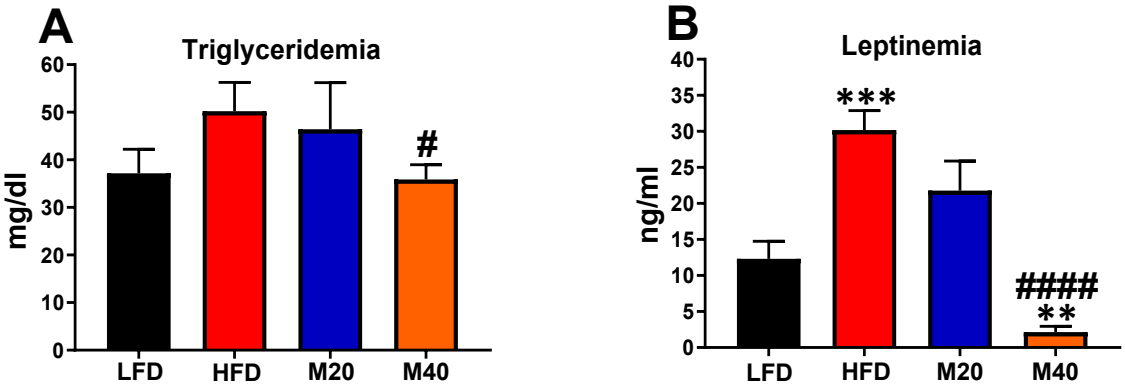
A
Triglyceridemia
mg/dl
60
50
40
30
20
10
0
#
LFD
HFD
M20
M40
B
Leptinemia
ng/ml
40
35
30
25
20
15
10
5
0
***
####
**
LFD
HFD
M20
M40

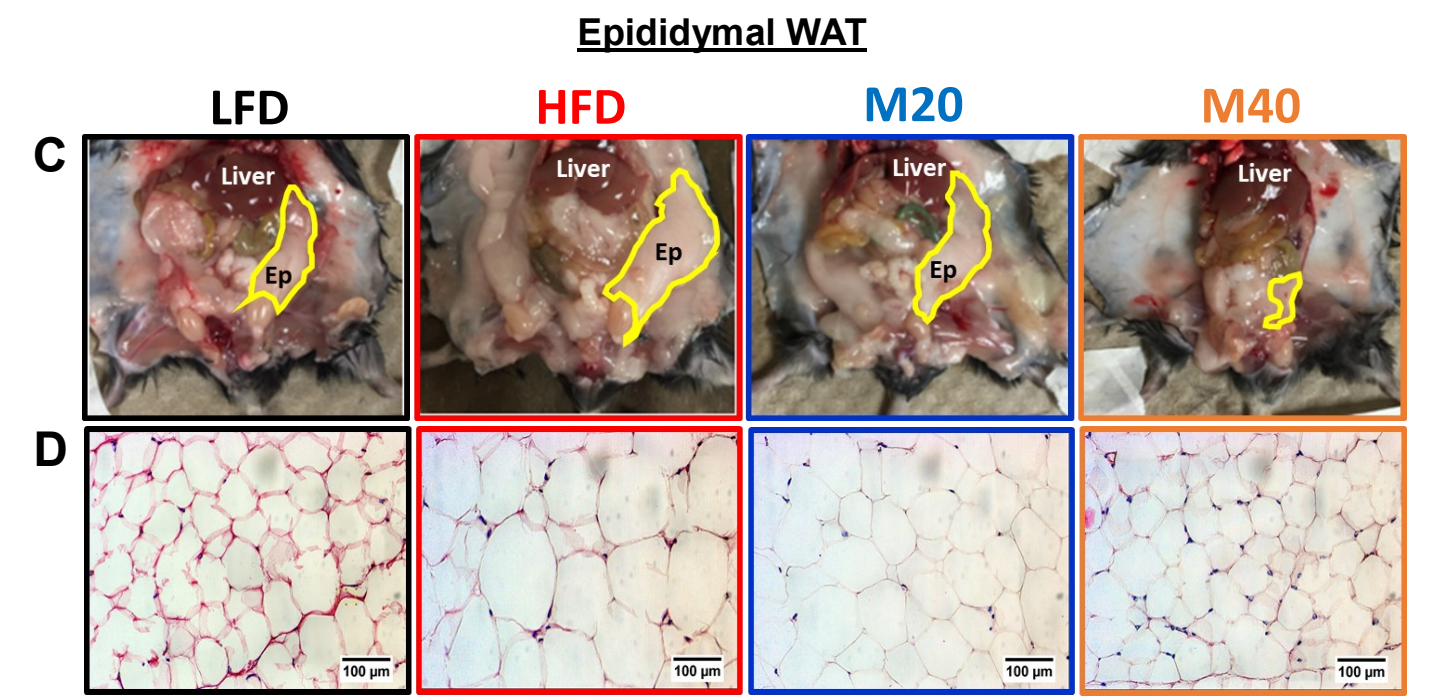
Epididymal WAT
LFD
HFD
M20
M40
C
Liver
Ep
D
100 µm

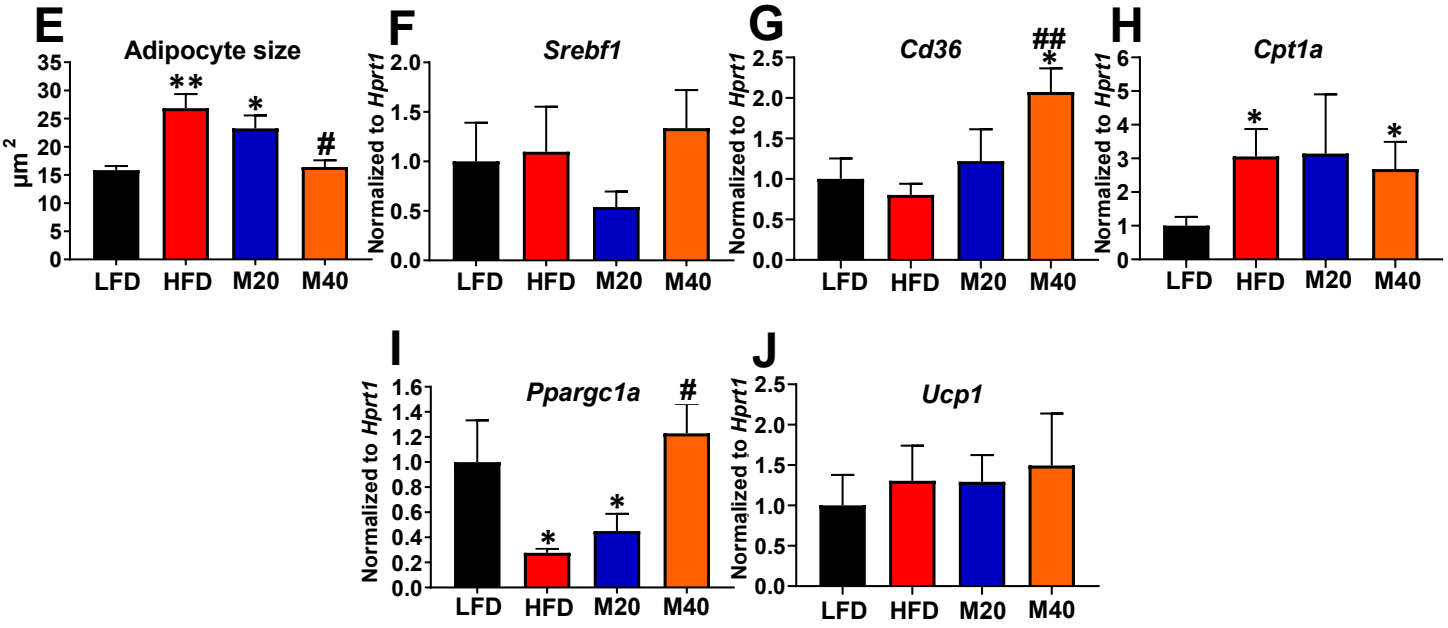
E
Adipocyte size
µm 2
35
30
25
20
15
10
5
0
**
*
#
LFD
HFD
M20
M40
F
Srebf1
Normalized to Hprt1
2.0
1.5
1.0
0.5
0.0
G
Cd36
##
*
2.5
2.0
1.5
1.0
0.5
0.0
H
Cpt1a
6
5
4
3
2
1
0
I
Ppargc1a
#
*
1.6
1.4
1.2
1.0
0.8
0.6
0.4
0.2
0.0
J
Ucp1
2.5
2.0
1.5
1.0
0.5
0.0

Figure 5

Subcutaneous WAT

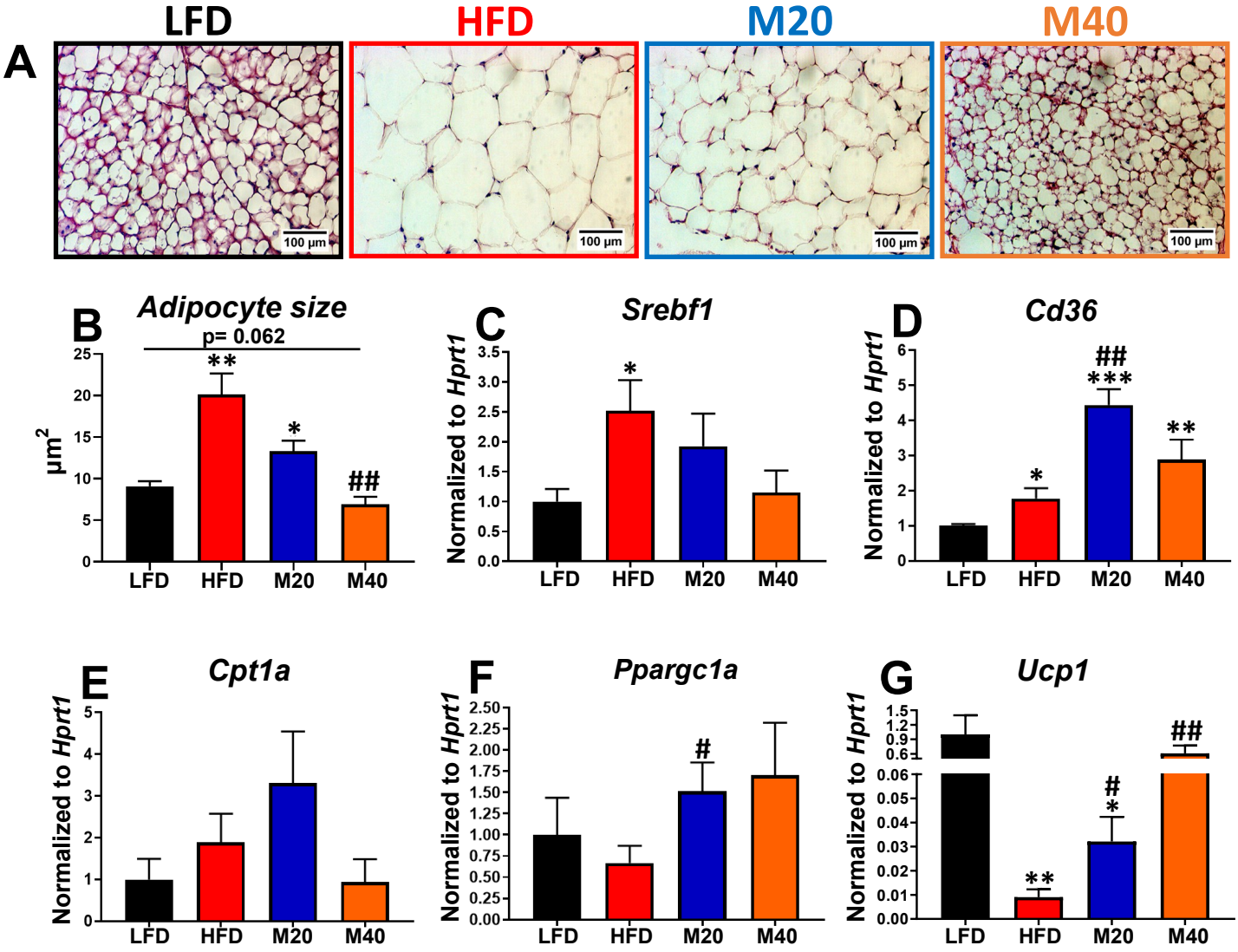

Figure 6

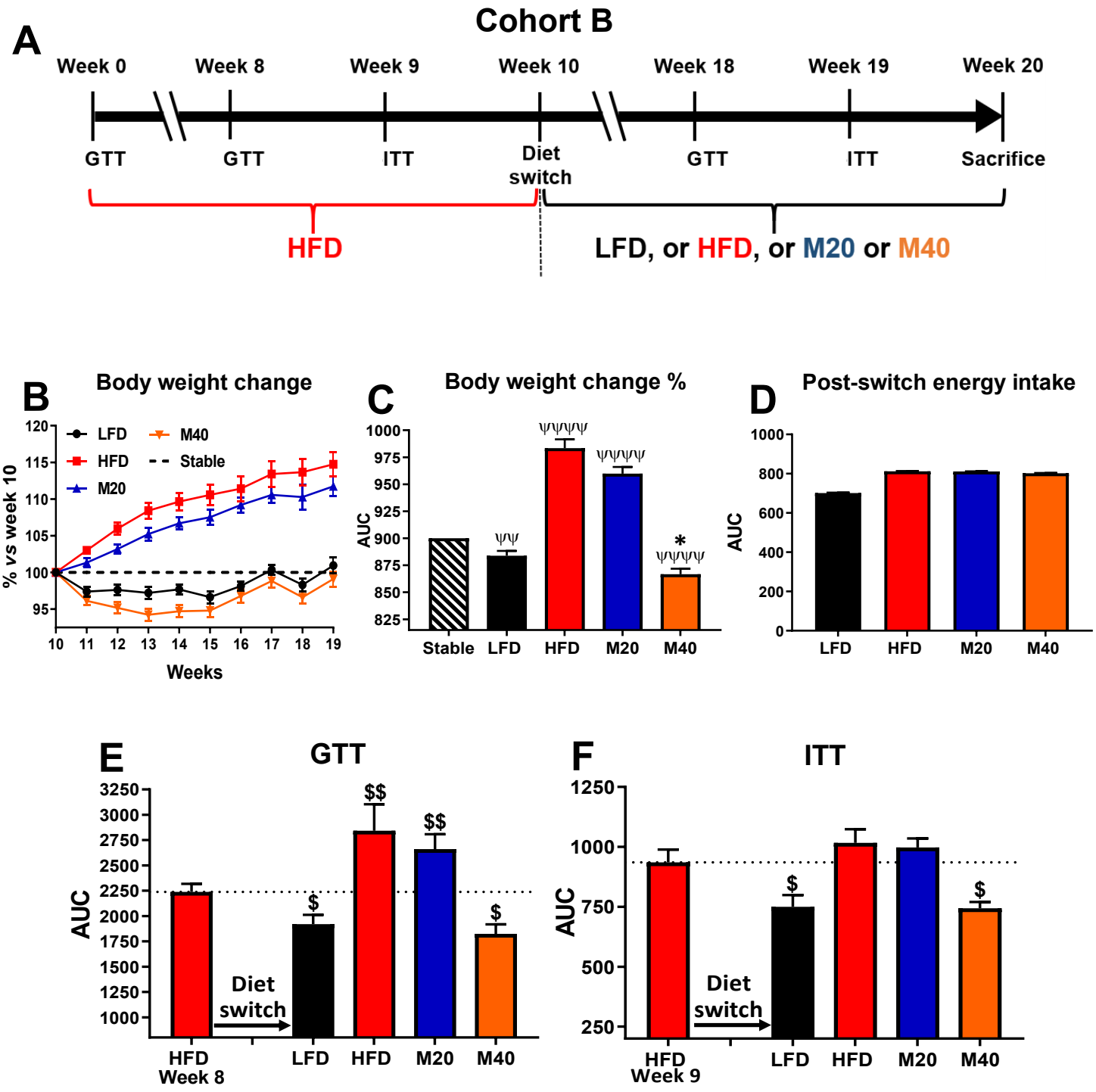
A
Cohort B
Week 0
Week 8
Week 9
Week 10
Week 18
Week 19
Week 20
GTT
GTT
ITT
Diet switch
GTT
ITT
Sacrifice
HFD
LFD, or HFD, or M20 or M40
B
Body weight change
LFD
HFD
M20
M40
Stable
% vs week 10
Weeks
C
Body weight change %
AUC
Stable
LFD
HFD
M20
M40
D
Post-switch energy intake
AUC
LFD
HFD
M20
M40
E
GTT
AUC
Diet switch
HFD Week 8
LFD
HFD
M20
M40
F
ITT
AUC
Diet switch
HFD Week 9
LFD
HFD
M20
M40

Figure 7

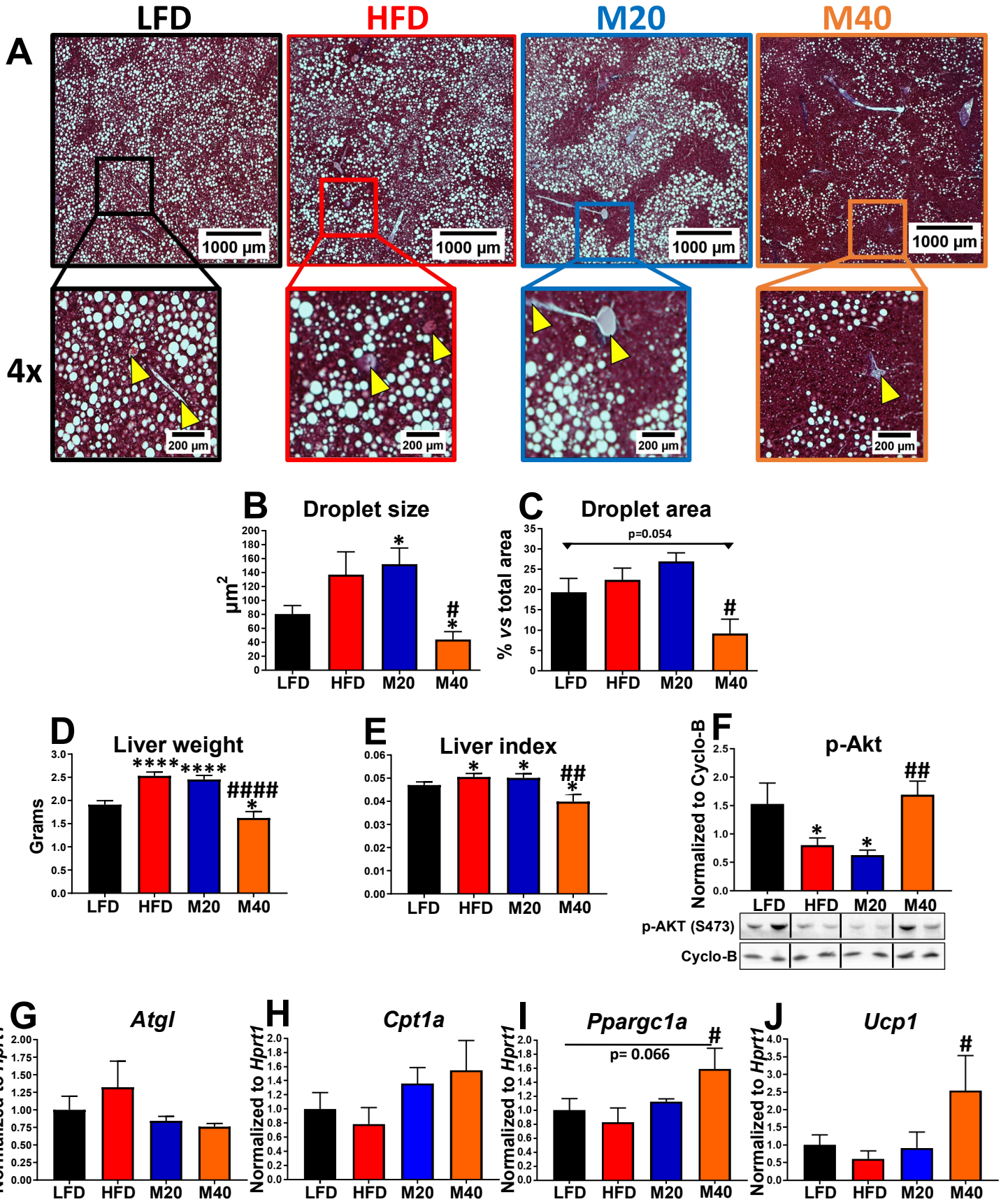
A
LFD
HFD
M20
M40
1000 µm
4x
200 µm
B
Droplet size
µm2
C
Droplet area
% vs total area
p=0.054
D
Liver weight
Grams
E
Liver index
F
p-Akt
Normalized to Cyclo-B
p-AKT (S473)
Cyclo-B
G
Atgl
H
Cpt1a
I
Ppargc1a
p= 0.066
J
Ucp1
Normalized to Hprt1
LFD
HFD
M20
M40

Figure 8

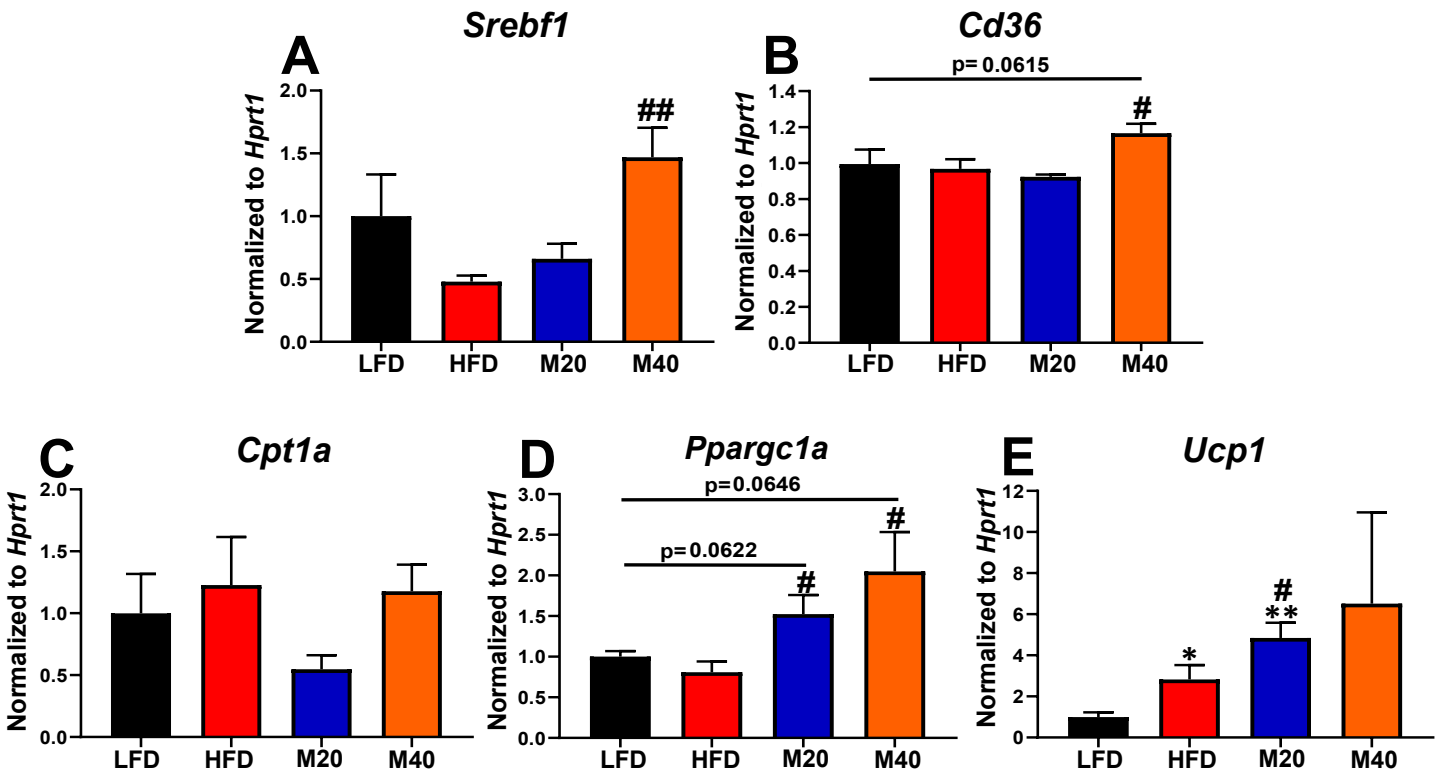
A
Srebf1
Normalized to Hprt1
2.0
1.5
1.0
0.5
0.0
##
LFD
HFD
M20
M40
B
Cd36
p= 0.0615
Normalized to Hprt1
1.4
1.2
1.0
0.8
0.6
0.4
0.2
0.0
#
LFD
HFD
M20
M40
C
Cpt1a
Normalized to Hprt1
2.0
1.5
1.0
0.5
0.0
LFD
HFD
M20
M40
D
Ppargc1a
p=0.0646
p=0.0622
Normalized to Hprt1
3.0
2.5
2.0
1.5
1.0
0.5
0.0
#
#
LFD
HFD
M20
M40
E
Ucp1
Normalized to Hprt1
12
10
8
6
4
2
0
*
#
**
LFD
HFD
M20
M40

Supplementary Figure 1

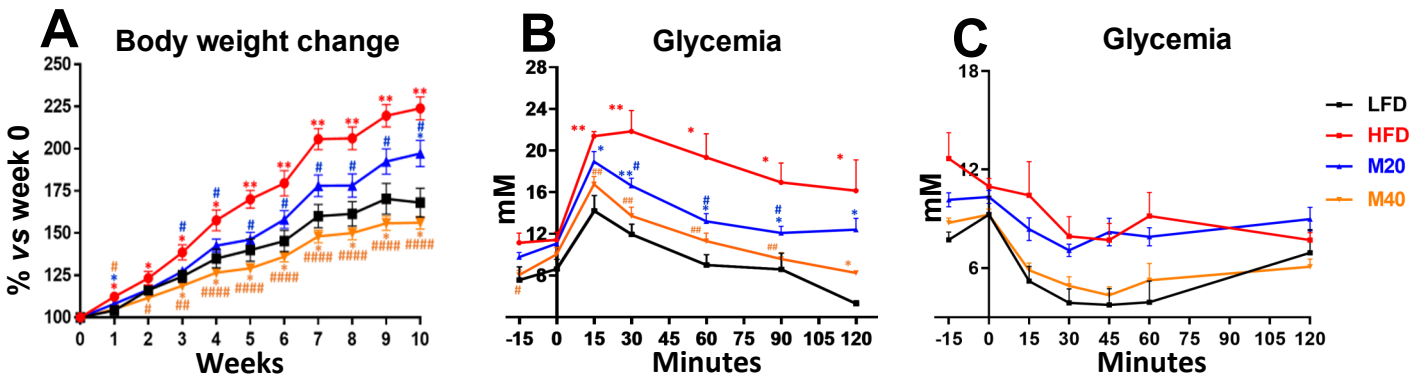

Supplementary Figure 2

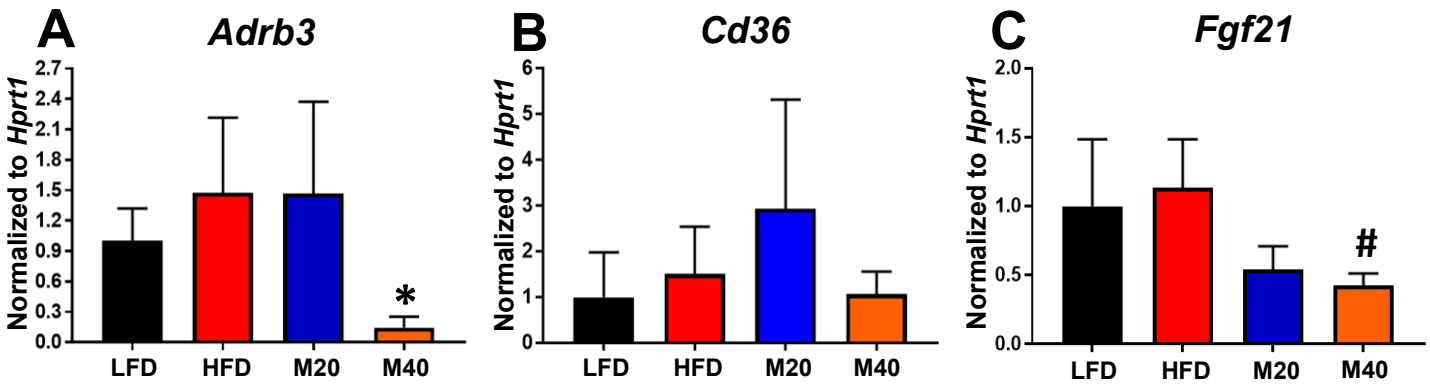

Supplementary Figure 3

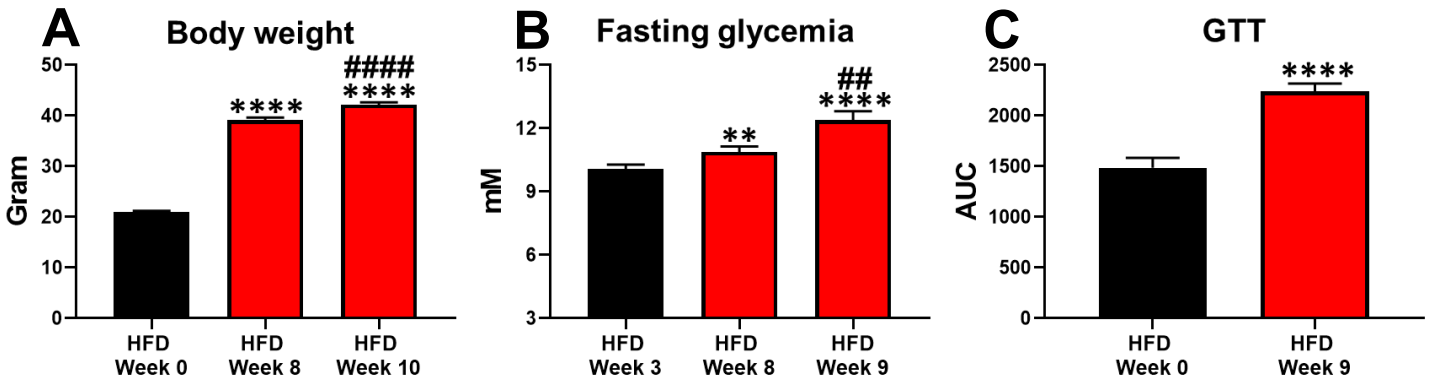

Supplementary Figure 4

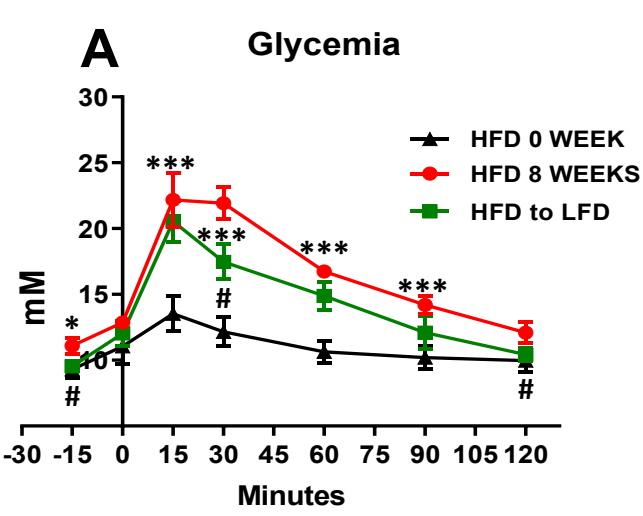

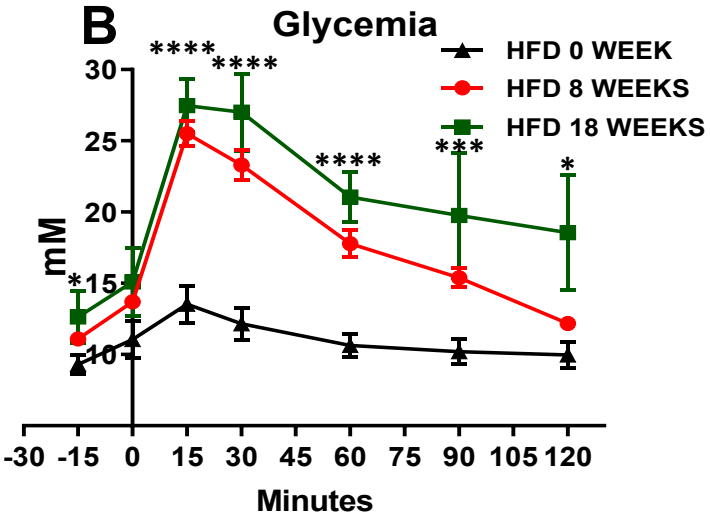

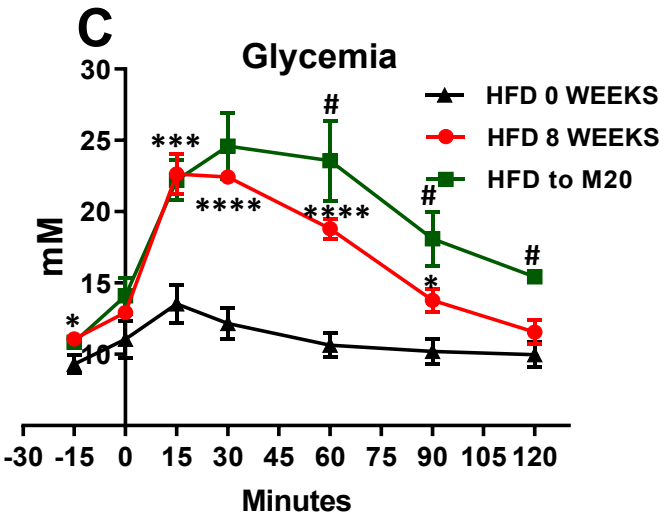

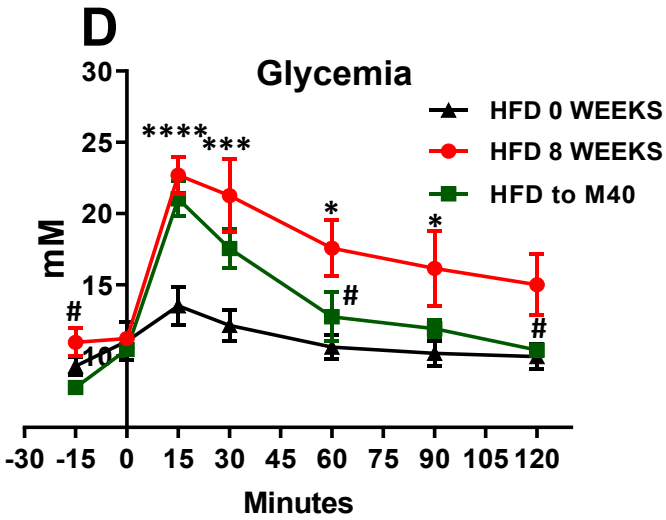

Supplementary Figure 5